phospho-ATM levels, p53 accumulation (Fig. 2(C)), and apoptotic cell death of myocytes as assessed by Bax/Bcl2 ratio and the number of TUNEL-positive cells (Figs. 2(C) and (D)). These data collectively suggest that doxorubicin treatment induces p53 accumulation via oxidative DNA damage-ATM pathway in cardiac myocytes.

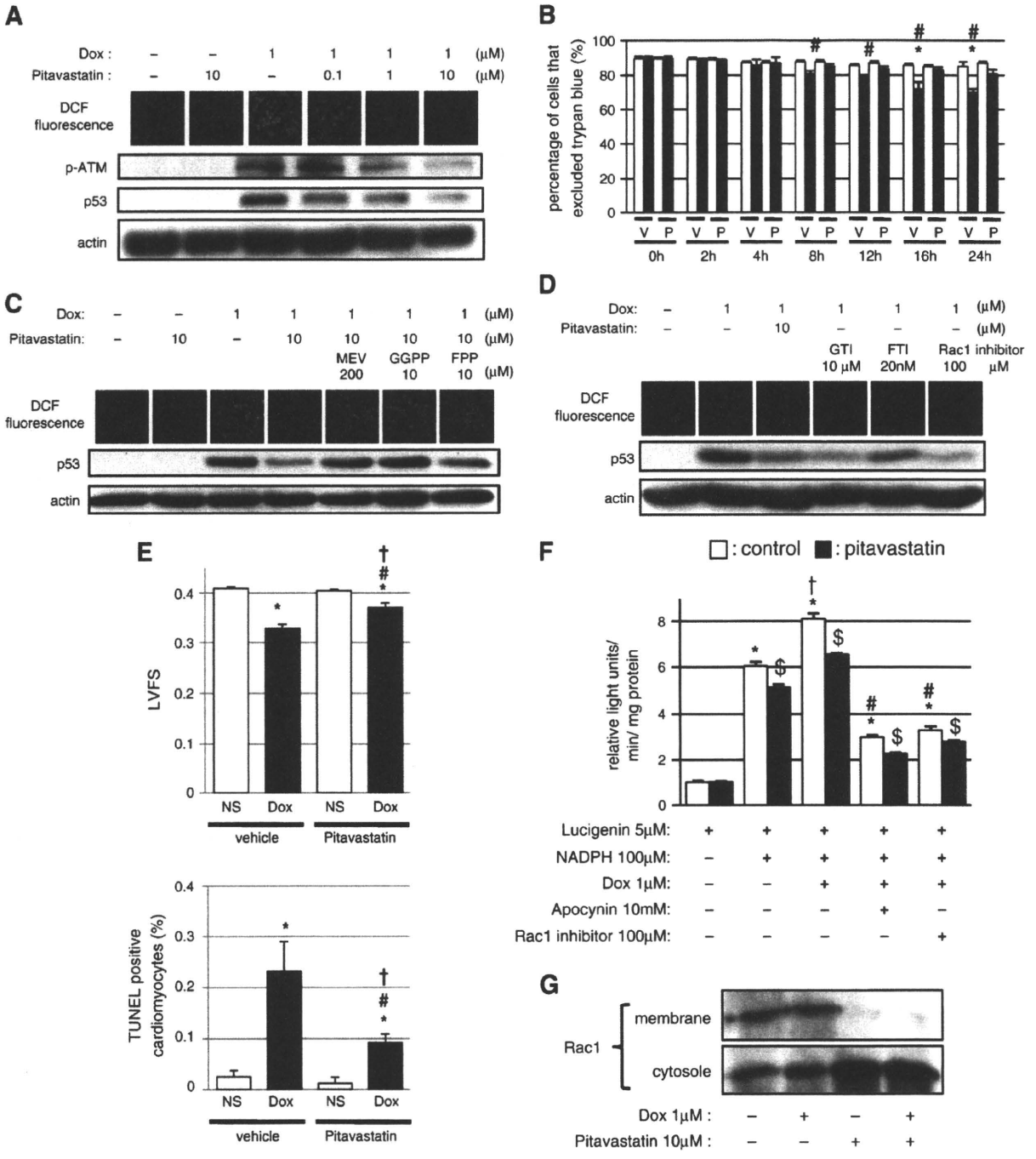

Fig. 4. Pitavastatin attenuates doxorubicin cardiotoxicity through its antioxidant effect involving Rac1 inhibition. (A) Pitavastatin attenuates doxorubicin-induced oxidative stress, ATM activation, and p53 accumulation in vitro. Oxidative stress was assessed by DCF fluorescence, and ATM activation and p53 accumulation were assessed by Western blot analysis. (B) Pitavastatin attenuates doxorubicin-induced myocyte death as assessed by trypan blue exclusion assay. White columns and black columns represent control (saline-treated) group and doxorubicin-treated group, and V and P represent vehicle and pitavastatin treatment, respectively. $^{\#}P<0.05$ vs vehicle-treated control group at the same time points; $^{*}P<0.05$ vs pitavastatin-treated doxorubicin group at the same time points. (C) Intermediate products of the mevalonate pathway reverse the beneficial effects of pitavastatin on doxorubicin cardiotoxicity. MEV, mevalonate. (D) GTI and Rac1 inhibitor but not FTI exhibit protective effects on doxorubicin cardiotoxicity. (E) Pitavastatin attenuates doxorubicin-induced cardiomyopathy. Top: left ventricular fractional shortening of mice treated with normal saline (NS) or doxorubicin (Dox). Mice were further divided into vehicle-treated group or pitavastatin-treated group. Bottom: number of TUNEL-positive cardiomyocytes 4 weeks after doxorubicin treatment. $^{*}P<0.05$ vs saline/vehicle-treated group; $^{\#}P<0.05$ vs saline/pitavastatin-treated group; $^{\dagger}P<0.05$ vs doxorubicin/vehicle-treated group. (F) Pitavastatin attenuates NADPH oxidase activity. White columns and black columns represent control (saline-treated) group and pitavastatin-treated group, respectively. $^{*}P<0.05$ vs lucigenin-treated control group; $^{\dagger}P<0.05$ vs lucigenin/NADPH-treated control group; $^{\#}P<0.05$ vs lucigenin/NADPH/doxorubicin-treated control group; $^{\$}P<0.05$ vs control group with the same treatment. (G) Pitavastatin inhibits translocation of Rac1 to plasma membrane. Molecular weight of Rac1 is 22 kDa.

3.2. Doxorubicin cardiotoxicity is mediated by p53-dependent cardiomyocyte apoptosis

We next examined the role of p53-dependent cardiomyocyte apoptosis in doxorubicin-induced cardiotoxicity in vivo. After chronic doxorubicin treatment, contractile function was impaired and apoptotic cardiomyocyte death was increased compared with vehicle treatment group in wild type mice (Fig. 3(A)). The deleterious effects of doxorubicin were attenuated in p53 heterozygous knockout mice, suggesting that p53 accumulation plays a causal role in doxorubicin cardiotoxicity (Fig. 3(B)). p53-induced cardiomyocyte apoptosis, myocardial ischemia, and mTOR inhibition have been implicated in the pathogenesis of various forms of heart failure [1,2,7,8]. However, doxorubicin cardiotoxicity was attenuated by cardiac-specific overexpression of anti-apoptotic protein Bcl-2 (Fig. 3(C)), whereas myocardial vessel density or myocyte size was not altered by chronic doxorubicin treatment (data not shown). Thus, doxorubicin cardiotoxicity is mediated by p53-dependent cardiomyocyte apoptosis.

3.3. Pitavastatin attenuates doxorubicin cardiotoxicity through its antioxidant effect involving Rac1 inhibition

Because oxidative stress is a critical inducer of p53 accumulation in the heart by doxorubicin and statins have been shown to have antioxidant effects, we examined whether pitavastatin exerts protective effects on doxorubicin cardiotoxicity. Pretreatment with pitavastatin attenuated doxorubicin-induced oxidative stress, ATM phosphorylation, p53 accumulation, and cardiomyocyte death (Figs. 4(A) and (B)). Statins are known to exert their lipid lowering-independent effects by inhibiting the synthesis of isoprenoids that are critical for posttranslational modification of a variety of proteins [9]. We therefore tested whether pitavastatin attenuates doxorubicin cardiotoxicity through the inhibition of mevalonate-dependent posttranslational protein modifications. Pretreatment with mevalonate, FPP, or GGPP reversed the beneficial effects of pitavastatin on doxorubicin-induced oxidative stress and p53 accumulation (Fig. 4(C)). Likewise, GTI but not FTI reduced doxorubicin-induced oxidative stress and p53 accumulation (Fig. 4(D)), suggesting that the inhibition of protein geranylgeranylation mediates the cardioprotective effects of pitavastatin. Because Rac1 is a major regulator of NADPH oxidase activity and activated by geranylgeranylation but not by farnesylation [14], we next examined the possible involvement of Rac1 in pitavastatin-mediated protective effects against doxorubicin. Indeed, treatment with a Rac1 inhibitor also attenuated doxorubicin-induced oxidative stress and p53 accumulation to the extent comparable with those of pitavastatin and GTI (Fig. 4(D)). Finally, treatment with pitavastatin significantly attenuated chronic doxorubicin treatment-induced cardiomyocyte apoptosis and contractile dysfunction in vivo (Fig. 4(E)), which is consistent with a recent report by others [23]. In cultured myocytes, doxorunbicin augmented NADPH oxidase activity, which was attenuated both by a NADPH oxidase assembly inhibitor (apocynin) and a Rac1 inhibitor (Fig. 4(F)). Furthermore, pitavastatin attenuated Rac1 activity as assessed by subcellular localization (Fig. 4(G)). These results collectively suggest that pitavastatin attenuates doxorubicin cardiotoxicity through its antioxidant effect involving Rac1 inhibition.

4. Discussion

4.1. Doxorubicin induces p53 accumulation in cardiac myocytes through oxidative DNA damage-ATM pathway

Several lines of evidence suggest that oxidative stress and p53 accumulation are involved in doxorubicin-induced cardiotoxicity [1,2]. Consistent with this notion, doxorubicin treatment induced oxidative stress and p53 accumulation both in vitro and in vivo, and reduction of oxidative stress by NAC treatment reduced doxorubicin-induced p53 accumulation in vitro. Because DNA damage is induced by doxorubicin and is a potent inducer of p53 in other cell types [21], we examined whether DNA damage mediates doxorubicin-induced p53 accumulation in cardiac myocytes. Indeed, doxorubicin treatment induced DNA damage and ATM activation, and an ATM kinase inhibitor wortmannin reduced p53 accumulation induced by doxorubicin. These findings are consistent with the notion that ATM activated by DNA damage phosphorylates and stabilizes p53 protein, and suggest that doxorubicin induces p53 accumulation via oxidative DNA damage-ATM pathway. However, it should be noted that p53 accumulation is not completely inhibited by treatment with NAC or wortmannin. It was also reported that the cardioprotective effects of antioxidants are not very remarkable in human clinical trials [24]. Thus, oxidative stress-independent mechanisms may also play a role in doxorubicin-induced p53 accumulation.

4.2. Chronic doxorubicin cardiotoxicity is mediated by p53-dependent cardiomyocyte apoptosis

Previous studies have shown that doxorubicin treatment induces p53 accumulation in the heart, and reduction of p53 activity attenuates deleterious effects of doxorubicin [5,6], suggesting that p53 plays a causal role in doxorubicin cardiotoxicity. Because doxorubicin-induced myocyte apoptosis was reduced by the inhibition of p53 activity, p53-dependent cardiomyocyte apoptosis has been thought to play a crucial role in doxorubicin cardiotoxicity. However, we have recently shown that p53 inhibits the action of hypoxia-inducible factor-1 (Hif-1) and Hif-1-dependent coronary angiogenesis in the heart under chronic pressure overload, leading to contractile dysfunction [7]. More recently, it was shown that p53-induced inhibition of mTOR activity mediates acute doxorubicin cardiotoxicity independently of cardiomyocyte apoptosis [8]. These results suggest that p53-dependent but apoptosis-independent mechanisms may be involved in the pathogenesis of doxorubicin cardiotoxicity. We therefore re-evaluated the role of cardiomyocyte apoptosis in doxorubicin cardiotoxicity using transgenic mice in which cardiomyocyte apoptosis is inhibited by the overexpression of Bcl-2 in the heart, and found that inhibition of myocardial apoptosis significantly improved contractile dysfunction induced by chronic doxorubicin treatment. We also found that doxorubicin treatment did not result in myocardial hypoxia or reduction in myocyte size. Thus, we conclude that chronic doxorubicin cardiotoxicity is mediated by p53-dependent cardiomyocyte apoptosis. These data collectively suggest that, although both acute and chronic doxorubicin cardiotoxicity are mediated by p53, the downstream effectors of p53 in these two situations may be partly distinct. This notion is supported by a transcriptome analysis of acute and chronic doxorubicin cardiotoxicity, in which a different set of genes were up- or down-regulated in the heart after acute and chronic doxorubicin treatment, respectively [25]. It should also be noted that in tumor cell lines, DNA damage induces both p53-dependent and p53-independent apoptosis [26]. Whether DNA damage-dependent p53-independent apoptosis plays a role in doxorubicin cardiotoxicity remains to be elucidated.

4.3. Pitavastatin attenuates doxorubicin cardiotoxicity by inhibiting Rac1 activity

HMG-CoA reductase inhibitors or statins are widely prescribed drugs that inhibit the rate-limiting enzyme for cholesterol synthesis in the liver and lower serum cholesterol levels. However, these drugs also exert cholesterol lowering-independent or pleiotropic effects, many of which are thought to be mediated by their ability to inhibit the synthesis of isoprenoid intermediates required for posttranslational protein modifications. Specifically, isoprenylation of small G proteins such as Ras, Rho or Rac are critical for their proper membrane localization and function, and statin-mediated inhibition of these small G proteins may play a role in the pleiotropic effects of statins. Indeed, our in vitro studies

using isoprenoid intermediates and pharmacological inhibitors strongly suggest that inhibition of Rac1 activation by pitavastatin plays a crucial role in the protective effects of pitavastatin on doxorubicin cardiotoxicity. Because Rac1 is a requisite component of NADPH oxidase, our findings collectively suggest that pitavastatin attenuates doxorubicin cardiotoxicity through its antioxidant effect involving Rac1 inhibition. It was previously shown that oxidative stress is implicated in cardiac hypertrophy and that statins attenuate myocardial hypertrophy through Rac1 inhibition [12], suggesting that similar mechanisms may be involved in the pathogenesis of cardiac hypertrophy and doxorubicin cardiotoxicity.

In summary, we have shown that doxorubicin cardiotoxicity is mediated by oxidative DNA damage-ATM-p53-apoptosis pathway in vitro and in vivo, and attenuated by pitavastatin through its antioxidant effect involving Rac1 inhibition. Further clinical studies are mandatory to determine whether statins are really cardioprotective in the setting of anticancer therapy using doxorubicin or related chemotherapeutic agents.

Acknowledgments

We thank Dr. Michael D. Schneider for Bcl-2 transgenic mice, and E. Fujita, R. Kobayashi, and Y. Ishiyama for technical assistance. This work was supported by grants from the Ministry of Education, Culture, Sports, Science and Technology to IK.

References

[1] Minotti G, Menna P, Salvatorelli E, Cairo G, Gianni L. Anthracyclines: molecular advances and pharmacologic developments in antitumor activity and cardiotoxicity. Pharmacol Rev 2004 Jun;56(2):185–229.
[2] Takemura G, Fujiwara H. Doxorubicin-induced cardiomyopathy from the cardiotoxic mechanisms to management. Prog Cardiovasc Dis 2007 Mar–Apr;49 (5):330–52.
[3] Yen HC, Oberley TD, Vichitbandha S, Ho YS, St Clair DK. The protective role of manganese superoxide dismutase against adriamycin-induced acute cardiac toxicity in transgenic mice. J Clin Invest 1996 Sep 1;98(5):1253–60.
[4] Sun X, Zhou Z, Kang YJ. Attenuation of doxorubicin chronic toxicity in metallothionein-overexpressing transgenic mouse heart. Cancer Res 2001 Apr 15;61(8): 3382–7.
[5] Liu X, Chua CC, Gao J, Chen Z, Landy CL, Hamdy R, et al. Pifithrin-alpha protects against doxorubicin-induced apoptosis and acute cardiotoxicity in mice. Am J Physiol Heart Circ Physiol 2004 Mar;286(3):H933–9.
[6] Shizukuda Y, Matoba S, Mian OY, Nguyen T, Hwang PM. Targeted disruption of p53 attenuates doxorubicin-induced cardiac toxicity in mice. Mol Cell Biochem 2005 May;273(1–2):25–32.
[7] Sano M, Minamino T, Toko H, Miyauchi H, Orimo M, Qin Y, et al. p53-induced inhibition of Hif-1 causes cardiac dysfunction during pressure overload. Nature 2007 Mar 22;446(7134):444–8.
[8] Zhu W, Soonpaa MH, Chen H, Shen W, Payne RM, Liechty EA, et al. Acute doxorubicin cardiotoxicity is associated with p53-induced inhibition of the mammalian target of rapamycin pathway. Circulation 2009 Jan 6;119(1):99–106.
[9] Mital S, Liao JK. Statins and the myocardium. Semin Vasc Med 2004 Nov;4(4): 377–84.
[10] Endres M, Laufs U, Huang Z, Nakamura T, Huang P, Moskowitz MA, et al. Stroke protection by 3-hydroxy-3-methylglutaryl (HMG)-CoA reductase inhibitors mediated by endothelial nitric oxide synthase. Proc Natl Acad Sci U S A 1998 Jul 21;95(15):8880–5.
[11] Lefer AM, Campbell B, Shin YK, Scalia R, Hayward R, Lefer DJ. Simvastatin preserves the ischemic-reperfused myocardium in normocholesterolemic rat hearts. Circulation 1999 Jul 13;100(2):178–84.
[12] Takemoto M, Node K, Nakagami H, Liao Y, Grimm M, Takemoto Y, et al. Statins as antioxidant therapy for preventing cardiac myocyte hypertrophy. J Clin Invest 2001 Nov;108(10):1429–37.
[13] Hasegawa H, Yamamoto R, Takano H, Mizukami M, Asakawa M, Nagai T, et al. 3-Hydroxy-3-methylglutaryl coenzyme A reductase inhibitors prevent the development of cardiac hypertrophy and heart failure in rats. J Mol Cell Cardiol 2003 Aug;35(8):953–60.
[14] Groemping Y, Rittinger K. Activation and assembly of the NADPH oxidase: a structural perspective. Biochem J 2005 Mar 15;386(Pt 3):401–16.
[15] Zou Y, Komuro I, Yamazaki T, Kudoh S, Uozumi H, Kadowaki T, et al. Both Gs and Gi proteins are critically involved in isoproterenol-induced cardiomyocyte hypertrophy. J Biol Chem 1999 Apr 2;274(14):9760–70.
[16] Tanaka M, Nakae S, Terry RD, Mokhtari GK, Gunawan F, Balsam LB, et al. Cardiomyocyte-specific Bcl-2 overexpression attenuates ischemia–reperfusion injury, immune response during acute rejection, and graft coronary artery disease. Blood 2004 Dec 1;104(12):3789–96.
[17] Li SY, Gomelsky M, Duan J, Zhang Z, Gomelsky L, Zhang X, et al. Overexpression of aldehyde dehydrogenase-2 (ALDH2) transgene prevents acetaldehyde-induced cell injury in human umbilical vein endothelial cells: role of ERK and p38 mitogen-activated protein kinase. J Biol Chem 2004 Mar 19;279(12):11244–52.
[18] Szocs K, Lassegue B, Sorescu D, Hilenski LL, Valppu L, Couse TL, et al. Upregulation of Nox-based NAD(P)H oxidases in restenosis after carotid injury. Arterioscler Thromb Vasc Biol 2002 Jan;22(1):21–7.
[19] Deng S, Kruger A, Kleschyov AL, Kalinowski L, Daiber A, Wojnowski L. Gp91phox-containing NAD(P)H oxidase increases superoxide formation by doxorubicin and NADPH. Free Radic Biol Med 2007 Feb 15;42(4):466–73.
[20] Spallarossa P, Garibaldi S, Altieri P, Fabbi P, Manca V, Nasti S, et al. Carvedilol prevents doxorubicin-induced free radical release and apoptosis in cardiomyocytes in vitro. J Mol Cell Cardiol 2004 Oct;37(4):837–46.
[21] L'Ecuyer T, Sanjeev S, Thomas R, Novak R, Das L, Campbell W, et al. DNA damage is an early event in doxorubicin-induced cardiac myocyte death. Am J Physiol Heart Circ Physiol 2006 Sep;291(3):H1273–80.
[22] Kurz EU, Douglas P, Lees-Miller SP. Doxorubicin activates ATM-dependent phosphorylation of multiple downstream targets in part through the generation of reactive oxygen species. J Biol Chem 2004 Dec 17;279(51):53272–81.
[23] Riad A, Bien S, Westermann D, Becher PM, Loya K, Landmesser U, et al. Pretreatment with statin attenuates the cardiotoxicity of Doxorubicin in mice. Cancer Res 2009 Jan 15;69(2):695–9.
[24] Ladas EJ, Jacobson JS, Kennedy DD, Teel K, Fleischauer A, Kelly KM. Antioxidants and cancer therapy: a systematic review. J Clin Oncol 2004 Feb 1;22(3):517–28.
[25] Yi X, Bekeredjian R, DeFilippis NJ, Siddiquee Z, Fernandez E, Shohet RV. Transcriptional analysis of doxorubicin-induced cardiotoxicity. Am J Physiol Heart Circ Physiol 2006 Mar;290(3):H1098–102.
[26] Roos WP, Kaina B. DNA damage-induced cell death by apoptosis. Trends Mol Med 2006 Sep;12(9):440–50.

Transplantation of cardiac progenitor cells ameliorates cardiac dysfunction after myocardial infarction in mice

Katsuhisa Matsuura,[1,2] Atsushi Honda,[1] Toshio Nagai,[3] Noritoshi Fukushima,[1] Koji Iwanaga,[3] Masakuni Tokunaga,[3] Tatsuya Shimizu,[2] Teruo Okano,[2] Hiroshi Kasanuki,[1] Nobuhisa Hagiwara,[1] and Issei Komuro[3]

[1]Department of Cardiology and [2]Institute of Advanced Biomedical Engineering and Science, Tokyo Women's Medical University, Tokyo, Japan.
[3]Department of Cardiovascular Science and Medicine, Chiba University Graduate School of Medicine, Chiba, Japan.

Cardiac progenitor cells are a potential source of cell therapy for heart failure. Although recent studies have shown that transplantation of cardiac stem/progenitor cells improves function of infarcted hearts, the precise mechanisms of the improvement in function remain poorly understood. The present study demonstrates that transplantation of sheets of clonally expanded stem cell antigen 1–positive (Sca-1–positive) cells (CPCs) ameliorates cardiac dysfunction after myocardial infarction in mice. CPC efficiently differentiated into cardiomyocytes and secreted various cytokines, including soluble VCAM-1 (sVCAM-1). Secreted sVCAM-1 induced migration of endothelial cells and CPCs and prevented cardiomyocyte death from oxidative stress through activation of Akt, ERK, and p38 MAPK. Treatment with antibodies specific for very late antigen-4 (VLA-4), a receptor of sVCAM-1, abolished the effects of CPC-derived conditioned medium on cardiomyocytes and CPCs in vitro and inhibited angiogenesis, CPC migration, and survival in vivo, which led to attenuation of improved cardiac function following transplantation of CPC sheets. These results suggest that CPC transplantation improves cardiac function after myocardial infarction through cardiomyocyte differentiation and paracrine mechanisms mediated via the sVCAM-1/VLA-4 signaling pathway.

Introduction

Accumulating evidence has suggested that myocardial regeneration is a promising therapy for various heart diseases (1). Recently, several groups, including our own, have reported that adult hearts contain cardiac stem/progenitor cells that can differentiate into functional cardiomyocytes in vitro and in vivo (2–6). Transplantation of cardiac stem/progenitor cells has been shown to improve cardiac function via newly formed cardiomyocytes and blood vessels (2, 7). On the other hand, it has been reported that when noncardiac stem cells are transplanted, paracrine factors play a major role in the improvement of cardiac function (8, 9). Several preclinical reports and clinical trials have demonstrated that intracoronary or intramyocardial injection of bone marrow–derived cells attenuates cardiac dysfunction following acute and chronic myocardial infarction (MI) (10–12). However, it is not known whether cardiac stem/progenitor cells are superior to other noncardiac stem/progenitor cells. Furthermore, it remains unclear to what extent paracrine effects or transdifferentiation of cardiac stem/progenitor cells contributes to beneficial effects on cardiac function.

Transplanted cells are the source of paracrine factors or newly formed cardiomyocytes, and the survival of grafted cells is a critical issue. The majority of the grafted cells have been reported to disappear within 1 week after transplantation when directly injected into ischemic hearts (9, 13), suggesting that alternative strategies to facilitate survival of grafted cells are required. We developed temperature-responsive culture dishes that were covalently grafted with the temperature-responsive polymer poly(*N*-isopropylacrylamide) (PIPAAm) (14). Lowering the temperature induces a rapid surface transition from hydrophobic (cell adhesive) to hydrophilic (non–cell adhesive), which results in the release of contiguous viable cell sheets with full preservation of cell-to-cell connections and adhesion proteins without using any enzymatic digestion (15). To date, cell sheet transplantations of skeletal myoblasts (16), mesenchymal stem cells derived from adipose tissue (17), and menstrual blood (18) have been reported to improve cardiac function in animal MI models. However, the precise mechanisms of the improvement, which include mutual interactions between host tissue and transplanted cells, remain poorly understood.

The present study demonstrates that transplanted cell sheets of clonally expanded stem cell antigen 1–positive (Sca-1–positive) cells (CPCs) differentiated into cardiomyocytes and vascular cells and prevented cardiac remodeling after MI. CPCs secreted soluble VCAM-1 (sVCAM-1), which facilitated engraftment and migration of CPCs from cell sheets into host myocardium and improved cardiac function after MI via angiogenic and cardioprotective effects mediated by paracrine mechanisms.

Results

Establishment and character of CPCs. Since primary isolated Sca-1–positive cells, which were derived from adult murine hearts, con-

Authorship note: Katsuhisa Matsuura and Atsushi Honda contributed equally to this work.

Conflict of interest: The authors have declared that no conflict of interest exists.

Nonstandard abbreviations used: ATMC, adipose tissue–derived mesenchymal cell; CM, conditioned medium; CPC, clonally expanded Sca-1–positive cell; FAK, focal adhesion kinase; FS, fractional shortening; IMDM, Iscove's Modified Dulbecco's Medium; LVDd, LV diastolic dimension; LVDs, LV systolic dimension; LVEDP, LV end-diastolic pressure; MI, myocardial infarction; miRNA, microRNA; RFP, red fluorescent protein; Sca-1, stem cell antigen 1; sVCAM-1, soluble VCAM-1; VLA-4, very late antigen-4.

Citation for this article: *J. Clin. Invest.* **119**:2204–2217 (2009). doi:10.1172/JCI37456.

sisted of several cell populations, including cardiac stem/progenitor cells, hematopoietic cells, and endothelial cells (ref. 4 and our unpublished observations), clonal cells were initially established from cardiac Sca-1–positive cells. A total of 10^4 primary isolated Sca-1–positive cells derived from adult murine hearts were plated onto 10-cm culture dishes. After repeated limited dilutions, clonal cell lines were established. The efficiency of cloning was approximately 0.1%. The clonal cells were expanded for more than 500 population doublings (Figure 1A). Flow cytometric analysis revealed that almost 100% of cells expressed Sca-1, CD29, and CD44, approximately 20% of cells expressed CD34, and no cells expressed CD31, CD45, and c-kit throughout the culture passages (Table 1 and Supplemental Figure 1; supplemental material available online with this article; doi:10.1172/JCI37456DS1), suggesting that the clonal cells were not homogenous. Under culture conditions of 80% confluency, the clonal cells expressed cardiac transcription factors, such as Nkx2.5 and GATA4 (Figure 1B), but not cardiac contractile proteins. These cell phenotypes remained unchanged throughout the culture passages. Gene profiles and cell-surface marker analyses revealed that CPCs were similar to primary isolated Sca-1–positive cells in analyses previously reported (4). Therefore, CPCs possessed features almost identical to those of intrinsic cardiac stem/progenitor cells. When CPCs were cultured under confluent conditions for 4 weeks, expression levels of Nkx2.5 and GATA4 were upregulated and expressions of myocyte enhancer factor 2C (MEF2C), atrial natriuretic peptide (ANP), β-myosin heavy chain (β-MHC), and sarcomeric α-actinin were detected at mRNA and protein levels (Figure 1, B and C). These results suggested that CPCs differentiated into immature cardiomyocytes in vitro. However, the cells did not exhibit spontaneous beating. To examine the cardiac differentiation potency of CPCs in vivo, 2.0×10^6 CPCs labeled with red fluorescent protein (RFP) were injected directly into the infarcted myocardium within 5 minutes after left coronary artery ligation. At 4 weeks after transplantation, several GATA4-expressing RFP^+ cells were recognized in the border areas and some RFP^+ cells expressed sarcomeric α-actinin in a fine striated pattern, which suggested that CPCs differentiated into mature cardiomyocytes in vivo (Figure 1, D and E). However, transplanted CPC-derived RFP expression in the infarcted heart was very weak 1 week after transplantation compared with immediately after transplantation (Supplemental Figure 2). These results suggest that direct intramyocardial injection is not an ideal method for efficient engraftment.

Cell sheet transplantation. To elucidate the functional benefits of CPC transplantation in the infarcted heart compared with effects of noncardiac stem/progenitor cells, cell sheet transplantation methods were utilized. RFP^+ CPCs or adipose tissue–derived mesenchymal cells (ATMCs) isolated from GFP mice were cultured on temperature-responsive culture dishes at 37°C. The monolayered cell sheet was collected by decreasing the temperature at which it was cultured to 20°C. Final cell counts and areas of monolayered cell sheets prior to transplantation were $2.0 \pm 0.2 \times 10^6$ cells and 80.1 ± 3.3 mm² in CPCs and $1.9 \pm 0.1 \times 10^6$ cells and 79.3 ± 2.0 mm² in ATMCs, respectively ($n = 5$). The mice were randomly assigned into 3 groups: mice transplanted with monolayered CPCs (CPC group), mice transplanted with monolayered ATMCs (ATMC group), and mice that were not transplanted (MI group). Within 5 minutes after left coronary artery ligation, monolayered CPC or ATMC sheets were transplanted over the infarcted area and cardiac function was examined by echocardiography every week. Echocardiographic analysis revealed that LV diastolic dimension (LVDd) and LV systolic dimension (LVDs) were significantly decreased at 4 weeks and fractional shortening (FS) was markedly improved 3 weeks after transplantation in the CPC group compared with the MI and ATMC groups. These results suggested that transplantation of CPC sheets inhibited cardiac remodeling and improved cardiac function following MI (Figure 2A). Furthermore, LV end-diastolic pressure (LVEDP) and +dp/dt, as determined by catheter, were markedly improved in the CPC group compared with the remaining 2 groups at 4 weeks (Figure 2B). In contrast, in the ATMC group, LVDs was significantly smaller and FS was better 1 week after transplantation compared with the MI and CPC groups. However, these favorable effects were not observed 2 weeks after transplantation, and cardiac remodeling and dysfunction progressed in a manner similar to that in the MI group (Figure 2A). The fibrotic area, which was evaluated by Masson trichrome staining 4 weeks after transplantation, was significantly smaller in the CPC group compared with the other 2 groups (Figure 3A). At 1 week after transplantation, more vWF-positive blood vessels were observed in the border area of the ATMC group than in the MI and CPC groups (Figure 3B). At 4 weeks, a greater number of vessels were detected in the CPC group than in the MI and ATMC groups (Figure 3C). Furthermore, when lectin perfusion assay was performed at 4 weeks, more lectin-positive blood vessels were detected in the border area of the CPC group compared with the remaining 2 groups (Supplemental Figure 4). In contrast, there were few inflammatory cells in the border area of each group at 4 weeks (Supplemental Figure 5).

Cell survival and differentiation. Immunohistochemical analysis showed that many transplanted CPCs were present in the middle of the LV wall, including the normal and injured areas (normal area, 28.3 ± 9.7 cells/mm²; injured area, 235.9 ± 75.1 cells/mm²), after 4 weeks (Figure 4, A–C). This suggested that CPCs migrated from the epicardial cell sheet into the ventricular myocardium following transplantation. Conversely, GFP^+ ATMCs were not observed in the myocardium (data not shown). Western blot analysis, using Abs against fluorescent proteins, revealed that approximately 20% of transplanted CPCs remained 4 weeks after transplantation, whereas only approximately 0.8% of transplanted ATMCs remained (Supplemental Figure 3). Furthermore, approximately 30% of RFP^+ cells expressed sarcomeric α-actinin in a fine striated pattern, and some RFP^+ cells also formed blood vessel structures (Figure 4, D–F). Because cardiomyocytes have the ability to fuse with surrounding noncardiomyocytes (19), the possibility that CPCs acquired cardiomyogenic features following fusion with existing cardiomyocytes was examined. When RFP^+ CPC sheets were transplanted into hearts of GFP mice immediately following MI, approximately half of the α-actinin–expressing cells expressed GFP in injured areas 4 weeks after transplantation (Supplemental Figure 6, A, B, and E). In the normal areas, all of the α-actinin–expressing RFP^+ cells expressed GFP (Supplemental Figure 6, C–E). To further ensure the occurrence of cell fusion, sheets of nonlabeled CPCs derived from male mice were transplanted into the infarcted hearts of female mice. At 4 weeks after transplantation, cells exhibiting a fine striated pattern possessed 3 X chromosomes and a Y chromosome in the nucleus (Supplemental Figure 7). These findings suggested that CPCs differentiated into cardiomyocytes via cell fusion–dependent and –independent mechanisms. Because approximately 20% of transplanted CPCs remained at 4 weeks (Supplemental Figure 3), approximately

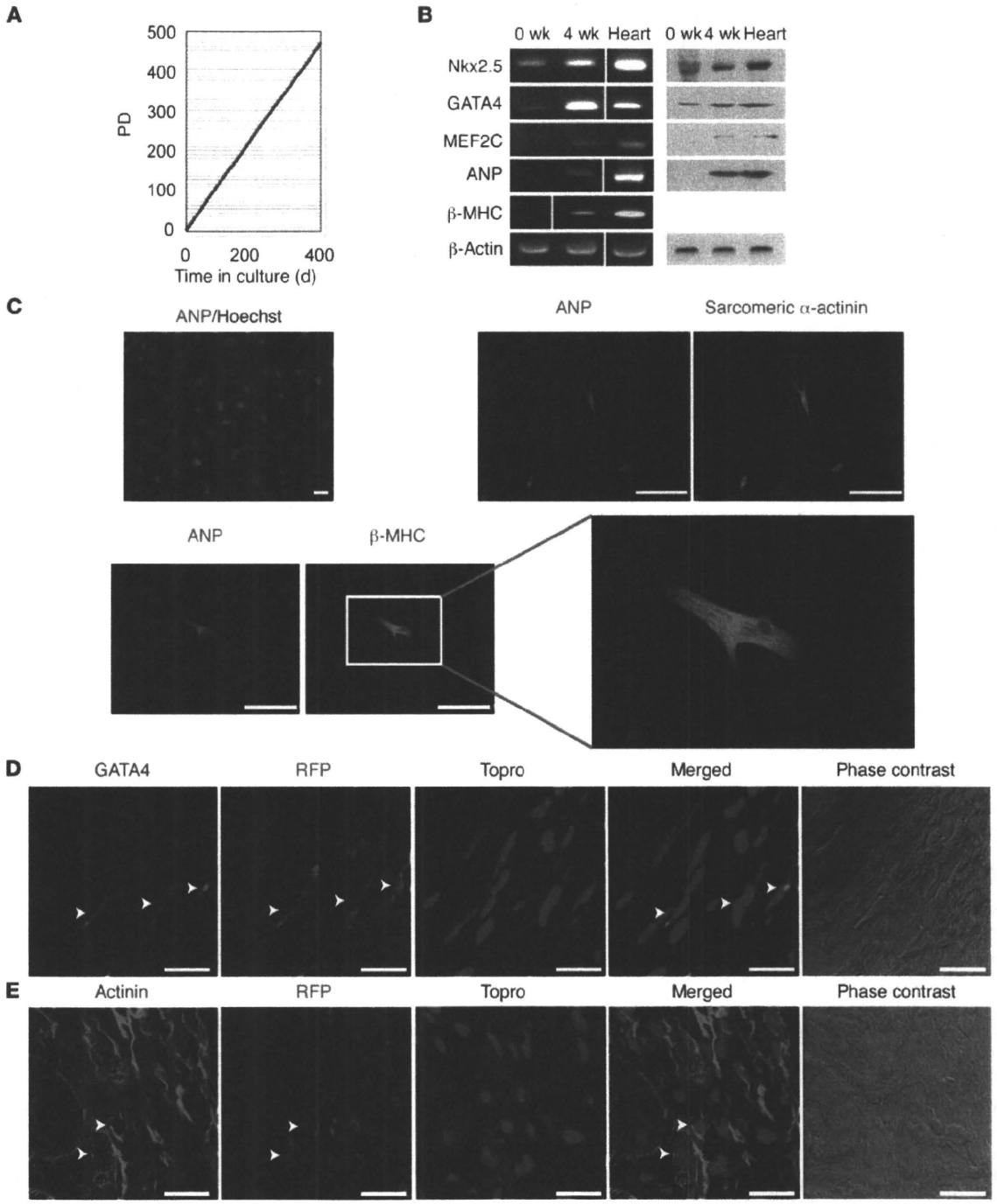

Figure 1

Character of CPCs. (**A**) CPCs were expanded more than 500 population doublings (P.D.) over a 1-year period. (**B** and **C**) Cardiac mRNA and protein expressions in CPCs. (**B**) Left panels show RT-PCR. Noncontiguous lanes from the same gel were spliced together into a composite band. The thin white line indicates the spliced point. Right panels show Western blot. (**C**) Immunofluorescent images of CPCs 4 weeks after starting culture under confluent conditions. Scale bars: 100 μm. (**D** and **E**) Confocal microscopic images of the infarcted heart 4 weeks after direct injection of RFP$^+$ CPCs. (**D**) GATA4-expressing RFP$^+$ cells (arrowheads) were recognized in the infarcted region. (**E**) Some RFP$^+$ cells (arrowheads) expressed sarcomeric α-actinin in the infarcted area. Scale bars: 5 μm.

4.0×10^5 out of approximately 2.0×10^6 transplanted CPCs were thought to survive and undergo engraftment. As approximately 30% of survived CPCs expressed cardiac contractile proteins (Figure 4, C and E), approximately 1.2×10^5 CPCs were estimated to differentiate into cardiomyocytes. Since approximately half of the cardiac protein-expressing cells resulted from cell fusion with

Table 1
The percentage of cell-surface antigens

	Sca-1	CD29	CD31	CD34	CD44	CD45	c-kit
P.D.10	99.8	99.9	0.1	15.6	100	0.5	0.4
P.D.100	95.5	99.7	0.3	42.8	100	0.2	0.3
P.D.200	99.8	100	0.1	45.5	100	0.1	0.1
P.D.300	99.8	99.9	0.2	15.5	99.9	0.4	0.2
P.D.400	100	100	0.3	27.5	100	0.3	0.4
P.D.500	99.9	99.9	0.1	15.4	100	0.5	0.5

existing cardiomyocytes (Supplemental Figure 6E), CPC sheet transplantation was estimated to create approximately 0.6×10^5 new cardiomyocytes in the entire heart. The number of cardiomyocytes in an adult murine heart has been estimated to be 3×10^6 (20). Therefore, approximately 5% of cardiomyocytes were regenerated and might have contributed to improved cardiac function by CPC sheet transplantation.

Secretion of growth factors. Recent reports have suggested that cell transplantation improves cardiac function after MI through the release of humoral factors (8, 9). Analyses of conditioned medium (CM) from CPCs and ATMCs using a cytokine Ab array revealed that sVCAM-1 was more abundant in CPCs, while VEGF was dominantly expressed in ATMCs (Table 2). Western blot analysis of whole-cell lysates and ELISA of CM confirmed altered expressions of VCAM-1/sVCAM-1 and VEGF between CPCs and ATMCs (Figure 5A). VCAM-1 expression was almost identical among the 3 groups at 1 week. However, at 4 weeks after transplantation, expression levels remained high in the CPC group compared with the other 2 groups (Figure 5B). Time course of VCAM-1 expression was consistent with improved cardiac function (Figure 2A). Conversely, VEGF expression was significantly upregulated at 1 week in the ATMC group compared with the other groups. However, at 4 weeks, expression levels were similar among the 3 groups (Figure 5B). This was consistent with observations that transplanted ATMC sheets improved cardiac function at 1 week but not at 4 weeks (Figure 2A). The concentrations of sVCAM-1 and VEGF in peripheral blood remained unchanged in all groups 1 and 4 weeks after transplantation (Supplemental Figure 8).

CPC-derived sVCAM-1–mediated angiogenesis and cardioprotective effects. CPC-derived CM and sVCAM-1 induced greater endothelial cell migration and tube formation compared with control medium (Figure 5, C and D). sVCAM-1–depleted CM, which was obtained from CPCs transfected with VCAM-1–specific microRNA (miRNA) plasmid vector (Supplemental Figure 9, A and B), induced significantly less endothelial cell migration (Figure 5C) and tube formation (Figure 5D) compared with CPC-derived CM. This suggested that angiogenic activity of CPC-derived CM was mediated at least in part by sVCAM-1. Subsequently, the protective

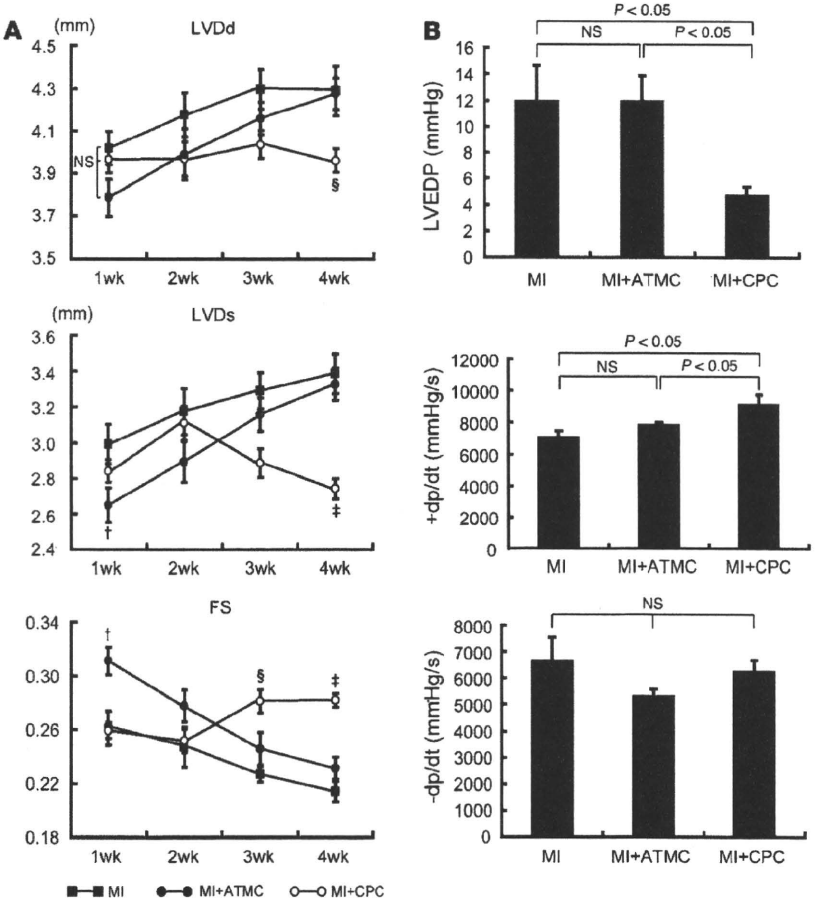

Figure 2
Effects of CPC sheet transplantation on cardiac function after MI. (**A**) Echocardiographic analysis. CPC sheet transplantation inhibited dilatation of LVDd and LVDs and improved FS 3 weeks later. ATMC transplantation inhibited dilatation of LVDs and FS reduction at 1 week, but not afterward. †$P < 0.05$ versus MI or MI plus CPCs ($n = 10$ per group). ‡$P < 0.01$ versus MI or MI plus ATMCs ($n = 10$ per group). §$P < 0.05$ versus MI or MI plus ATMCs ($n = 10$ per group). (**B**) Catheterization analysis at 4 weeks after transplantation. CPC sheet transplantation improved LVEDP and +dp/dt compared with that in the MI or MI plus ATMC groups ($n = 5$). Data are shown as mean ± SEM.

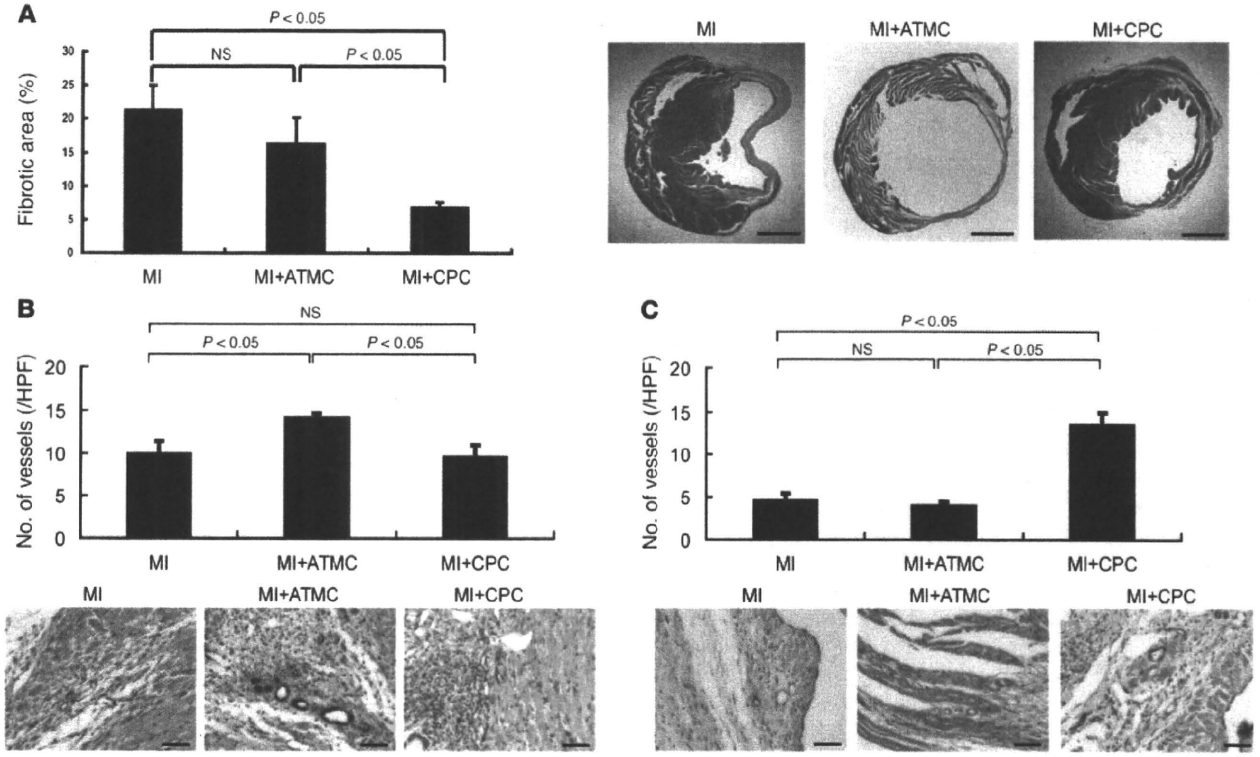

Figure 3

Immunohistochemical analysis of transplanted hearts. (**A**) Masson trichrome staining. The fibrotic area at 4 weeks after transplantation was calculated and is shown in the graph (n = 6). Lower panels show representative images. Scale bars: 1 mm. (**B** and **C**) Endothelial cells were identified by immunohistochemical staining with anti-vWF Ab in the border zone of the infarcted hearts 1 week (**B**) and 4 weeks (**C**) after transplantation. Lower panels show representative images. The vessel number was quantified and is depicted in the graph (n = 6). HPF, high-power field. Scale bars: 100 μm. Data are shown as mean + SEM.

effects of CPC-derived CM and sVCAM-1 on cardiomyocytes were analyzed. When cardiomyocytes were pretreated with CPC-derived CM or sVCAM-1, H_2O_2-induced damage of cardiomyocytes was significantly reduced (Figure 6A). The cardioprotective effects of CPC-derived CM were abolished by pretreatment of cardiomyocytes with Abs against very late antigen-4 (VLA-4, also known as $\alpha_4\beta_1$ integrin), a principal coreceptor of sVCAM-1 (Figure 6A), or sVCAM-1–depleted CM (Figure 6B). These results suggested a crucial role for sVCAM-1/VLA-4 in cardiomyocyte survival.

Integrin-mediated signals influence cardioprotective effects of sVCAM-1. Integrin-mediated signaling induces cell migration and survival by activating various kinases, such as focal adhesion kinase (FAK), Akt, ERK1/2, and p38 MAPK (21, 22). CPC-derived CM and sVCAM-1 induced phosphorylation and activation of FAK, Akt, ERK, and p38 MAPK in neonatal rat cardiomyocytes (Figure 6, C and E). When cardiomyocytes were pretreated with inhibitors of Akt, PI3K (wortmannin), p38 MAPK (SB203580), or ERK (PD98059), the cardioprotective effects of CPC-derived CM and sVCAM-1 were significantly inhibited (Figure 6, D and F). When cardiomyocytes were pretreated with anti–VLA-4 Abs prior to culturing in CPC-derived CM, phosphorylation of FAK, Akt, and ERK but not p38 MAPK was inhibited (Figure 6E). This suggests that the protective effects of CPC-derived CM on cardiomyocytes were achieved through sVCAM-1/VLA-4–mediated activation of Akt and ERK as well as VLA-4–independent activation of p38 MAPK.

sVCAM-1–induced migration of CPCs. Because a large number of transplanted CPCs migrated from the epicardial cell sheet to the ventricular myocardium following transplantation (Figure 4A), the effects of CPC-derived CM and sVCAM-1 on CPC migration were analyzed. When treated with CPC-derived CM or sVCAM-1, CPC migration was promoted, and anti–VLA-4 Abs or sVCAM-1 depletion markedly inhibited CM-induced migration of CPCs (Figure 6G). When CPCs were treated with sVCAM-1, phospho–p38 MAPK expression was significantly increased. However, expression of phospho-Akt and phospho-ERK remained unchanged. Phosphorylation of p38 MAPK was significantly inhibited by anti–VLA-4 Ab treatment (Figure 6H), which suggested that CPCs activated p38 MAPK through VLA-4. SB203580 inhibited CPC-derived CM- and sVCAM-1–induced CPC migration compared with the control (Figure 6I). These findings suggest that CPCs secreted sVCAM-1 and induced CPC migration via the VLA-4/p38 MAPK signaling pathway. Moreover, when VCAM-1 expression was downregulated, CPC viability was significantly decreased and apoptosis increased (Supplemental Figure 10), suggesting that VCAM-1 might be important for CPC survival.

VLA-4 signaling plays a crucial role in the beneficial effects of CPC sheet transplantation. The present findings suggest that CPC-secreted sVCAM-1 induced angiogenesis as well as CPC migration and survival and protected cardiomyocytes via VLA-4 in vitro. Subsequently, VLA-4 signaling was analyzed to determine its role in improved

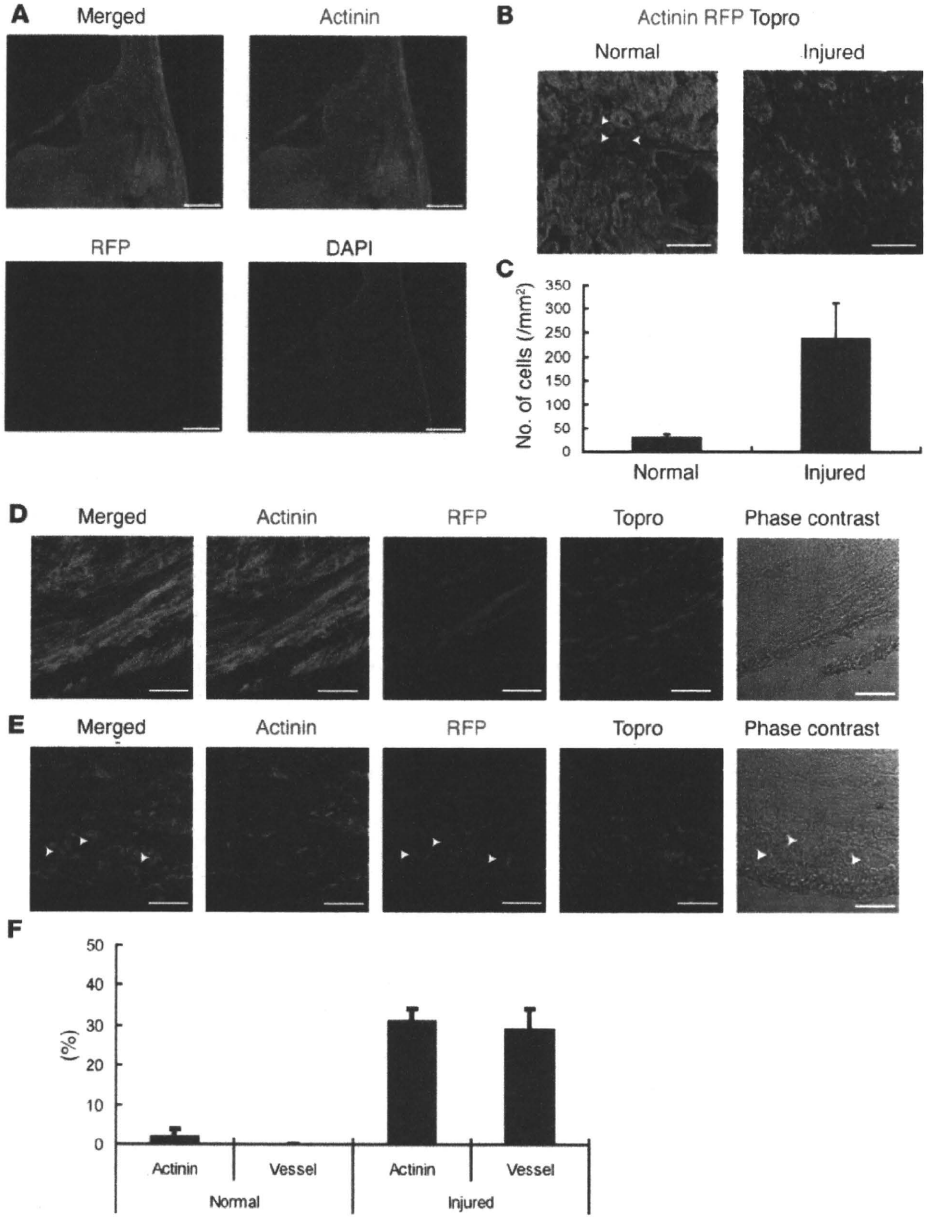

Figure 4
Cell survival and differentiation of transplanted cells. (**A**) Fluorescent microscopic images of infarcted heart 4 weeks after RFP+ CPC sheet transplantation. Left sides of panels show endocardial area. Right sides of panels show epicardial area. Scale bars: 250 μm. (**B**) Confocal microscopic images of infarcted heart 4 weeks after CPC sheet transplantation (sarcomeric α-actinin, green; RFP, red; Topro, blue; yellow in merged images). Left panel shows normal area. Right panel shows injured area. Arrowheads indicate RFP+ cells. Scale bars: 5 μm. (**C**) Number of RFP+ cells were quantified and shown in the graph (n = 5). (**D** and **E**) Transplanted RFP+ cells expressed sarcomeric α-actinin in a fine striated pattern (**D**) and formed vessel structures around α-actinin–positive myocardium (**E**). Nuclei were stained with Topro. Arrowheads indicate vessel structures. Scale bars: 5 μm. (**F**) Percentages of α-actinin–positive cells or vessel structure–forming cells in existing RFP+ cells were calculated and shown in the graph (n = 5). Data are shown as mean + SEM.

cardiac function following transplantation of CPC sheets. Because echocardiographic analysis revealed improved cardiac function 3 weeks after transplantation (Figure 2A), i.p. injection of anti–VLA-4 Abs was performed daily from 2 to 3 weeks after CPC sheet transplantation. At 4 weeks after transplantation, injection of anti–VLA-4 Abs significantly attenuated the beneficial effects of CPC sheet transplantation on cardiac function, fibrosis, and angiogenesis (Figure 7, A–D). The number of RFP+ CPCs in the infarcted area was also markedly decreased following treatment with anti–VLA-4 Abs (Figure 7E). In contrast, anti–VLA-4 Ab treatment did not affect cardiac function, fibrotic area, or blood vessel number in nontransplanted MI mice (Supplemental Figure 11). These findings suggest that CPC sheet transplantation improved cardiac function of infarcted hearts through VLA-4–mediated angiogenesis as well as survival and migration of transplanted CPCs.

Discussion

The present study reports that CPC sheet transplantation inhibited cardiac remodeling and restored cardiac function after MI by increasing the number of blood vessels and cardiomyocytes in the injured area. sVCAM-1 was identified as one of the dominant paracrine factors in CPCs and was shown to induce angiogenesis, cardioprotection, and CPC migration and survival through the VLA-4 signaling pathway. Therefore, sVCAM-1 plays a critical role in improved cardiac function following MI.

CPC transplantation restored cardiac function and angiogenic activity and prevented cardiac remodeling 4 weeks after transplantation. In contrast, ATMC transplantation attenuated cardiac dysfunction and enhanced angiogenesis transiently, and cardiac remodeling progressed at 4 weeks. These findings suggest varying cell survival rates (Supplemental Figure 3) and

Table 2
Results of cytokine Ab array

Cytokine	Fold increase
CPC	
VCAM-1	130.1
MIP-1γ	23.4
TIMP-1	8.0
IL-6	7.0
GM-CSF	6.0
IL-17	5.8
IL-5	5.3
KC	5.2
IFN-γ	5.2
IL-10	5.2
IL-12 p40/p70	4.8
IL-4	4.6
SDF-1α	4.5
IL-2	4.5
IL-12 p70	4.0
TNFα	3.9
MIP-3β	3.8
MIG	3.6
IL-9	3.1
MCP1	3.1
Osteopontin	2.1
ATMC	
MIP-1γ	135.7
KC	43.6
VCAM-1	22.4
RANTES	13.6
TIMP-1	11.9
IL-6	9.8
LIX	6.3
CXCL16	6.1
IL-17	5.6
GM-CSF	5.4
IL-2	4.8
IL-5	4.8
IL-4	4.3
IL-12 p70	4.2
IFN-γ	3.8
IL-10	3.6
IL-12 p40/p70	3.5
IL-9	3.4
Eotaxin	3.4
VEGF	3.2
TNFα	2.9
MCP1	2.9
MIP-3β	2.8
Osteopontin	2.5
MIG	2.4
CRG-2	2.2
SDF-1α	2.1

Each number indicates the fold increase of cytokine expression compared with the negative control. Serum-depleted medium was used as a negative control. SDF-1α, stromal cell–derived factor-1α; MIP-1γ, macrophage inflammatory protein-1γ; KC, keratinocyte-derived chemokine; TIMP-1 tissue inhibitor of metalloproteinase 1; LIX, LPS-induced chemokine; MCP1, monocyte chemotactic protein-1; MIG, monokine induced by gamma; CRT-2, cytokine-responsive gene-2.

distinct protein expression profiles (Figure 5B) in CPCs and ATMCs in the transplanted areas.

Through direct comparison of the protein expression profiles of CPCs and ATMCs, sVCAM-1 was identified as one of the predominantly expressed CPC-derived paracrine factors. VCAM-1, a 110-kDa transmembrane glycoprotein, is detected in various cells, including endothelial and bone marrow stromal cells (23). A soluble form of VCAM-1 has been reported to be shed from VCAM-1 on the cell surface by proteases, including TNF-α–converting enzyme (24). TNF-α–converting enzyme has also been reported to be elevated in the myocardium in heart failure (25) and to be required for fetal murine cardiac development and modeling (26). sVCAM-1 induces migration of endothelial cells through VLA-4 (21, 27, 28). The present study demonstrates that CM from VCAM-1–knocked-down CPCs did not induce endothelial migration, tube formation, cardioprotection, or CPC migration. Anti–VLA-4 Ab treatment abolished the protective effects of CPC-derived CM on cardiomyocytes and migration of CPCs and attenuated improved cardiac function following CPC sheet transplantation. This suggests that sVCAM-1 is a major paracrine factor of cardioprotection. VLA-4 is an integrin dimer that is composed of CD49d (α_4) and CD29 (β_1). Although studies have shown that the β_1 integrin signaling cascade regulates migration, differentiation, and death of various types of cells, such as endothelial cells, cardiomyocytes, and epidermal and hematopoietic stem cells (29–31), the role of sVCAM-1–mediated VLA-4 signaling in stem/progenitor cells remains elusive.

CPC-derived CM and sVCAM-1 phosphorylated several integrin-related downstream signaling molecules, such as Akt, ERK, and p38 MAPK, in cardiomyocytes. Consistent with previous studies, which indicated that Akt and ERK are critical for growth and survival of cardiomyocytes (32, 33), this study showed that promotion of cardiomyocyte survival by CPC-derived CM and sVCAM-1 was regulated through VLA-4–mediated activation of Akt and ERK. Furthermore, migration of CPCs, almost all of which expressed CD29 (β_1 integrin; Supplemental Figure 1), was facilitated via the VLA-4/p38 MAPK signaling pathway. VCAM-1–knockout mice and α_4 integrin–null mice have been shown to exhibit embryonic lethality, which was partly attributed to impaired epicardium formation surrounding the ventricular and atrial chambers, which suggests that VCAM-1/α_4 integrin signaling is critical for heart development (34, 35). In the present study, anti–VLA-4 Ab treatment reduced survival of transplanted CPCs. Furthermore, when VCAM-1 of CPCs was downregulated by specific miRNA, CPC viability was reduced and apoptosis was increased (Supplemental Figure 10), which suggests that VCAM-1–mediated signaling is also important for CPC survival. Since transplanted CPCs are the sources of not only paracrine factors but also newly formed cardiomyocytes, VCAM-1–mediated paracrine effects might also contribute to the cardiomyogenesis of CPCs through improved engraftment. A recent study has suggested that adult cardiac stem cells express α_4 and β_1 integrin in the niches (36). However, the role of α_4 and β_1 integrins is not fully understood. Since adult mammalian cardiomyocytes have been reported to be refreshed by endogenous stem cells after injury (37), our results suggest that sVCAM-1 secreted from transplanted CPCs promoted migration and self renewal of not only transplanted CPCs, but also endogenous cardiac stem/progenitor cells, through α_4 and β_1 integrin.

VCAM-1 is known as an inflammatory mediator, and increased sVCAM-1 in plasma has been reported following acute MI (38). During acute-phase MI, infiltrating leukocytes release cytokines,

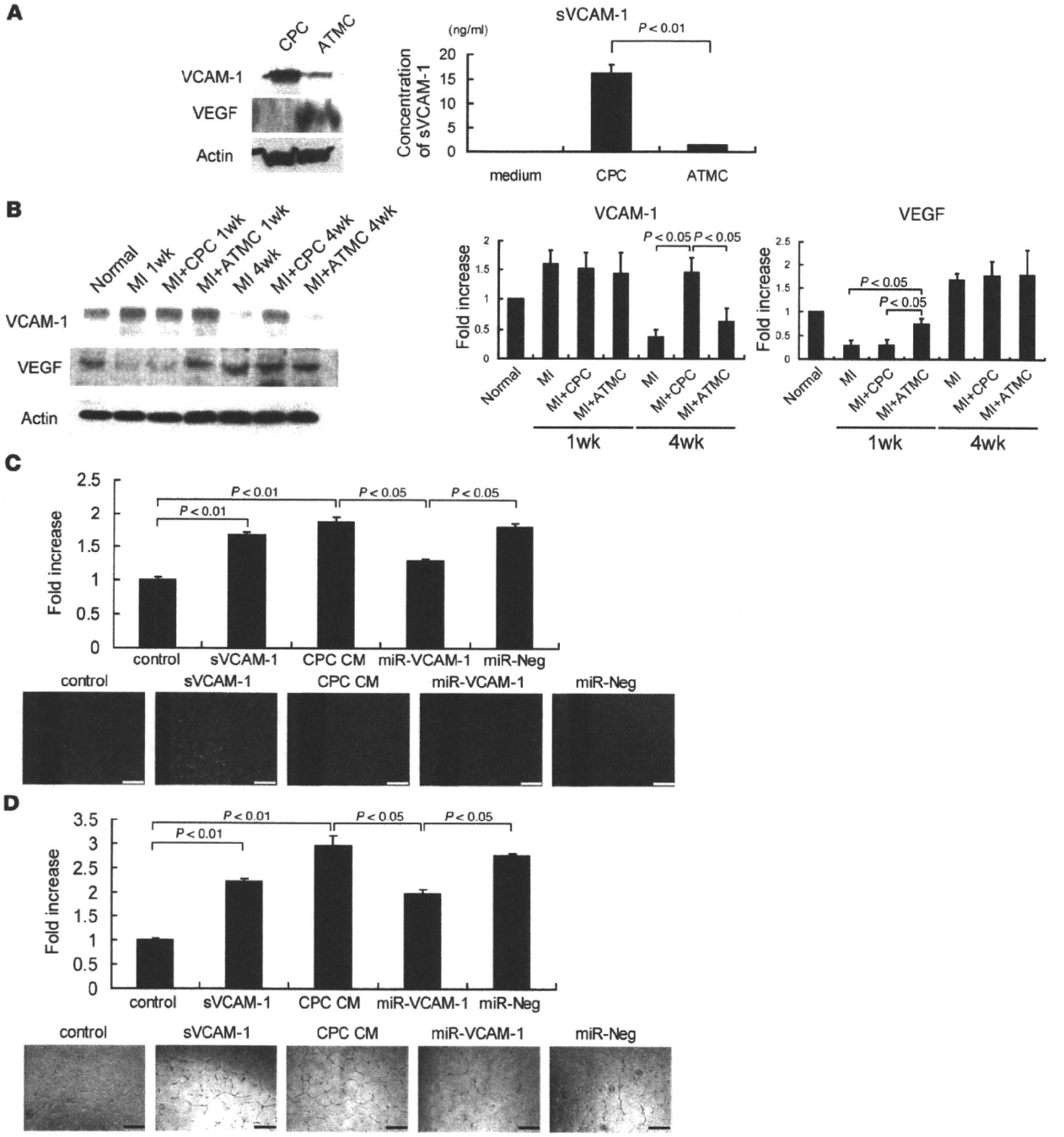

Figure 5

Secreted factor–mediated angiogenesis. (**A**) Left panel shows Western blot analysis results using whole-cell lysates of cultured CPCs and ATMCs. Right panel shows the results of sVCAM-1 ELISA using CM from cultured CPCs and ATMCs ($n = 3$). (**B**) Western blot analysis results of VCAM-1 and VEGF expression in heart after MI. Normal heart was used as a control. Left panel shows representative images. Right panels show quantification results of VCAM-1 and VEGF expression ($n = 3$). (**C**) Scratch-wound assay. CPC-derived CM enhanced endothelial migration ($n = 3$). Lower panels show representative images ($n = 3$). Scale bars: 500 μm. (**D**) CPC-derived CM enhanced endothelial tube formation. Tube length was quantified and is shown in the graph ($n = 3$). Lower panels show representative images. Scale bars: 500 μm. miR, miRNA. Data are shown as mean + SEM.

which activate VCAM-1 expression and promote leukocyte transmigration. In the present study, increased VCAM-1 expression in myocardium was observed in each group 1 week after MI/transplantation, when many inflammatory cells were also observed (data not shown). At 4 weeks, however, VCAM-1 expression remained upregulated in the CPC group despite few inflammatory

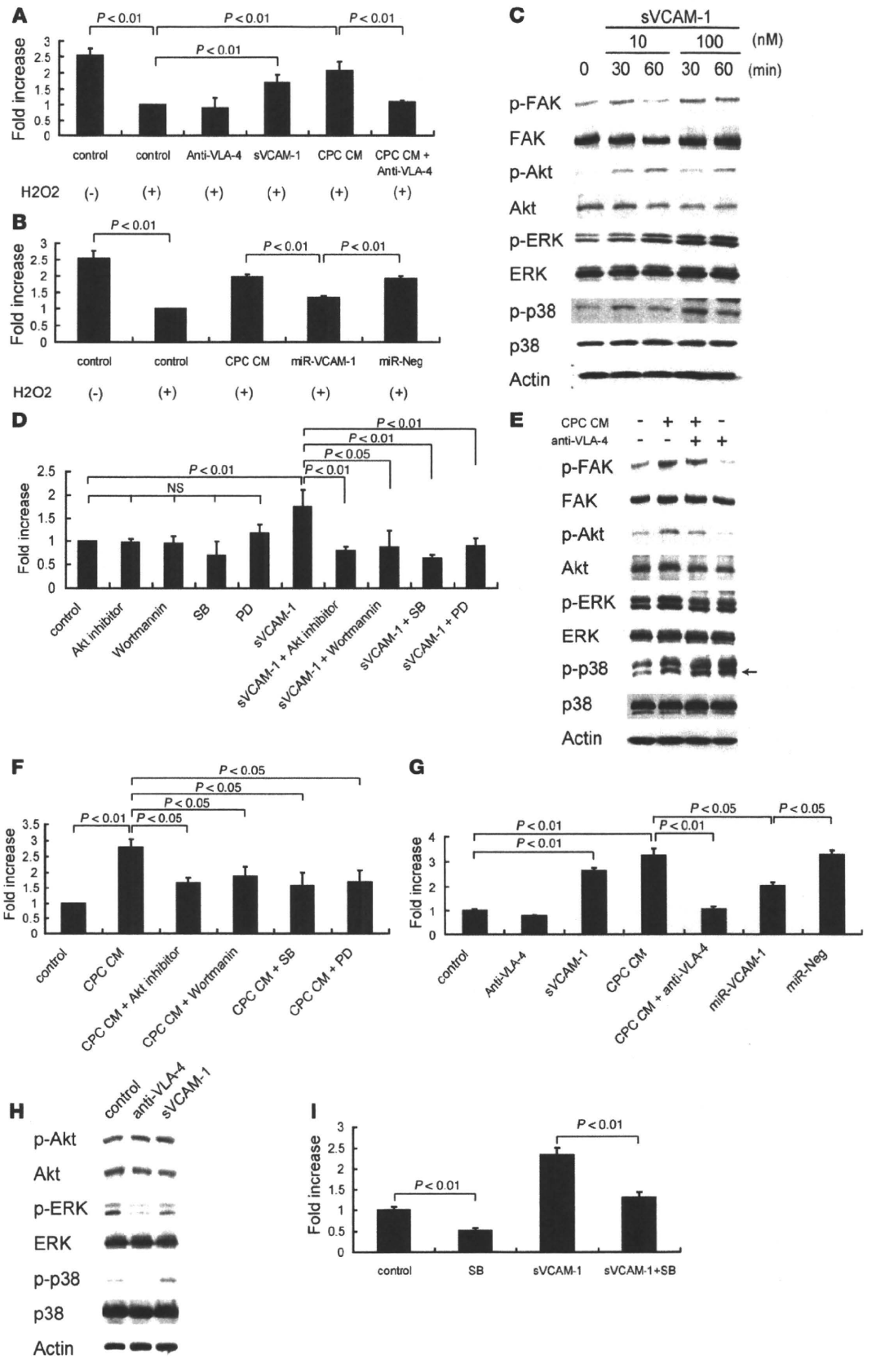
A
P < 0.01
P < 0.01
P < 0.01
P < 0.01
Fold increase
control
control
Anti-VLA-4
sVCAM-1
CPC CM
CPC CM + Anti-VLA-4
H2O2 (-) (+) (+) (+) (+) (+)
B
P < 0.01
P < 0.01
P < 0.01
Fold increase
control
control
CPC CM
miR-VCAM-1
miR-Neg
H2O2 (-) (+) (+) (+) (+)
C
sVCAM-1
10
100
(nM)
0 30 60 30 60 (min)
p-FAK
FAK
p-Akt
Akt
p-ERK
ERK
p-p38
p38
Actin
D
P < 0.01
P < 0.01
P < 0.05
P < 0.01
P < 0.01
NS
Fold increase
control
Akt inhibitor
Wortmannin
SB
PD
sVCAM-1
sVCAM-1 + Akt inhibitor
sVCAM-1 + Wortmannin
sVCAM-1 + SB
sVCAM-1 + PD
E
CPC CM - + + -
anti-VLA-4 - - + +
p-FAK
FAK
p-Akt
Akt
p-ERK
ERK
p-p38
p38
Actin
F
P < 0.05
P < 0.05
P < 0.05
P < 0.01
P < 0.05
Fold increase
control
CPC CM
CPC CM + Akt inhibitor
CPC CM + Wortmanin
CPC CM + SB
CPC CM + PD
G
P < 0.05
P < 0.05
P < 0.01
P < 0.01
P < 0.01
Fold increase
control
Anti-VLA-4
sVCAM-1
CPC CM
CPC CM + anti-VLA-4
miR-VCAM-1
miR-Neg
H
control
anti-VLA-4
sVCAM-1
p-Akt
Akt
p-ERK
ERK
p-p38
p38
Actin
I
P < 0.01
P < 0.01
Fold increase
control
SB
sVCAM-1
sVCAM-1+SB

Figure 6
sVCAM-1–mediated cardioprotective effects and CPC migration. (**A** and **B**) Cardiomyocyte viability following treatment with H_2O_2 was measured by MTT assay (n = 3). IgG isotype Abs were used as a control (**A**). (**C**) sVCAM-1 induced phosphorylation of FAK, Akt, ERK, and p38 MAPK in a dose-dependent manner. (**D**) Cardiomyocyte viability following treatment with H_2O_2 was measured by MTT assay (n = 4). SB, SB2035800; PD, PD98059. (**E**) CPC-derived CM induced phosphorylation of FAK, Akt, ERK, and p38 MAPK. Anti–VLA-4 Abs inhibited phosphorylation of FAK, Akt, and ERK induced by CPC-derived CM, but not phosphorylation of p38 MAPK. Arrow indicates appropriate size of phosphorylated p38 MAPK. (**F**) Cardiomyocyte viability following treatment with H_2O_2 was measured by MTT assay (n = 4). (**G** and **I**) CPC migration was measured using the scratch wound assay (n = 3). IgG isotype Ab was used as a control (**G**). (**H**) Anti–VLA-4 Abs inhibited phosphorylation of ERK and p38 MAPK of CPCs, but not Akt. Activity of p38 MAPK, but not Akt or ERK, was upregulated by sVCAM-1 treatment. Data are shown as mean + SEM.

cells in the infarcted area (Supplemental Figure 5). Furthermore, peripheral blood concentrations of sVCAM-1 were similar between groups 1 and 4 weeks after transplantation, which suggested that VCAM-1 expression in the transplanted heart was derived from CPC sheets, rather than circulating cells in the peripheral blood. VCAM-1 and its receptor, VLA-4, are important for fusion between hematopoietic progenitor cells and cardiomyocytes (39), and Oh et al. have reported that approximately 50% of cardiac protein-expressing transplanted cells arise from fusion with existing cardiomyocytes (3), which suggests that VCAM-1 mediates fusion between CPCs and dormant cardiomyocytes.

The present study compared transplanted cell survival between cell sheet transplantation and direct cell injection (Supplemental Figures 2 and 3). At 1 week after cell sheet transplantation, approximately 40% of cells survived (Supplemental Figure 3), while only 10% of cells survived after direct cell injection (Supplemental Figure 2). Immediately following transplantation, RFP expression in the heart was similar between cell sheet transplantation and direct cell injection, which suggested that the initial transplantation efficiency was the same. These findings indicate that cell sheet transplantation was superior to direct injection into the myocardium.

Many reports have demonstrated that endogenous cardiac stem/progenitor cells or bone marrow–derived cells mobilize to the infarcted area after injury and recruit additional cells through a feedback mechanism (40, 41). As shown in Table 2, CPCs expressed several chemokines, including stromal cell–derived factor-1 (SDF-1), which recruits bone marrow–derived cells to the infarcted myocardium (42). Therefore, CPC sheet transplantation may induce migration of bone marrow–derived cells to the infarcted heart, thereby improving cardiac function. Recently, anti-α_4 integrin Ab treatment was shown to improve cardiac function 2 weeks after MI by inhibiting interactions between bone marrow cells and their niches and promoting bone marrow cell migration and vasculogenesis (43). In the present study, anti–VLA-4 Ab treatment significantly attenuated improved cardiac function and angiogenesis following CPC sheet transplantation. Moreover, anti–VLA-4 Ab treatment did not affect cardiac function, fibrotic area, or blood vessel number in nontransplanted MI mice (Supplemental Figure 11). These findings suggest that bone marrow cells from their niches do not significantly contribute to the beneficial effects of CPC sheet transplantation.

There were a few limitations to the present study. The CPCs used in the experiments exhibited gene expression patterns similar to those of freshly isolated cardiac Sca-1–positive cells. However, profiles associated with proliferation, migration, and cardiomyocyte differentiation may not be the same. HUVECs were employed in endothelial migration and tube formation assays in vitro, and there might be differences between HUVECs and cardiac endothelial cells. Nevertheless, CPC sheet-mediated transplantation might be superior to the combination of other cell sources and tissue engineering methods. Improved survival of transplanted CPCs, in combination with several growth factors (44, 45), or multilayered cell sheets (46) might improve the beneficial effects of CPC sheet transplantation.

The present study identified the VCAM-1/VLA-4 signaling pathway as an important mechanism for CPC transplantation–mediated improved cardiac function. However, other paracrine factors, including thymosin β4 (47), have also been reported to contribute to cardiac repair following MI. Therefore, multiple mechanisms and mutual crosstalk might be involved in cell sheet transplantation to improve cardiac function. It remains to be determined which mechanisms are the most important and should be improved.

Methods

Animals. Wild-type mice (C57BL/6J) were purchased from Japan SLC. Adult GFP transgenic mice (C57BL/6J) were a gift from Masaru Okabe, Osaka University (Osaka, Japan). Neonatal Wistar rats (0 to 1 day old) were purchased from Saitama Experimental Animals Supply. All protocols were approved by the Institutional Animal Care and Use Committee of Tokyo Women's Medical University and Chiba University.

Reagents. FITC-conjugated anti-CD29, PE-conjugated anti-Sca-1, anti-CD44, and anti-c-kit Abs were purchased from eBioscience. PE-conjugated anti-CD31, anti-CD34, and anti-CD45 Abs were purchased from BD Biosciences – Pharmingen. The following Abs were used for immunostaining and Western blot analysis: mouse monoclonal anti-sarcomeric α-actinin, mouse monoclonal anti-β-actin (Sigma-Aldrich), rat monoclonal anti–VLA-4, mouse monoclonal anti-β-myosin heavy chain (anti-β-MHC) (Chemicon; Millipore), goat polyclonal anti-Nkx2.5, goat polyclonal anti-GATA4, rabbit polyclonal anti-atrial natriuretic peptide (anti-ANP), rabbit polyclonal anti-VEGF, goat polyclonal anti-Akt, rabbit polyclonal anti-FAK (Santa Cruz Biotechnology Inc.), rabbit polyclonal anti-GFP, rabbit polyclonal anti-RFP (MBL International Corp.), rabbit polyclonal anti-VCAM-1 (R&D Systems), rabbit polyclonal anti-vWF (Dako), rabbit polyclonal anti-myocyte enhancer factor 2C (anti-MEF2C), rabbit polyclonal anti-phospho Akt (Ser473), rabbit polyclonal anti-phospho p38 MAPK (Thr180/Tyr182), rabbit polyclonal anti-p38 MAPK, rabbit polyclonal anti-phospho ERK1/2, rabbit polyclonal anti-ERK1/2 (Cell Signaling Technology), and rabbit monoclonal anti-phospho FAK (Y397; Invitrogen). Secondary Abs were purchased from Jackson ImmunoResearch Laboratories Inc. Unless otherwise specified, reagents were purchased from Sigma-Aldrich.

Cell isolation. Sca-1–positive cells were isolated from an adult (10 weeks old) wild-type, male mouse, as described previously (4). Isolated cells (1×10^4) were harvested on a 10-cm Primaria dish (BD Falcon) in Iscove's Modified Dulbecco's Medium (IMDM) (Invitrogen) supplemented with 10% FBS and penicillin/streptomycin at 37°C in humid air with 5% CO_2. One month after starting culture, several colonies were recognizable. Each of these colonies was collected using a cloning cup and reseeding to a new 10-cm Primaria dish. After repeating this process 2 more times, a clonal cell line was established.

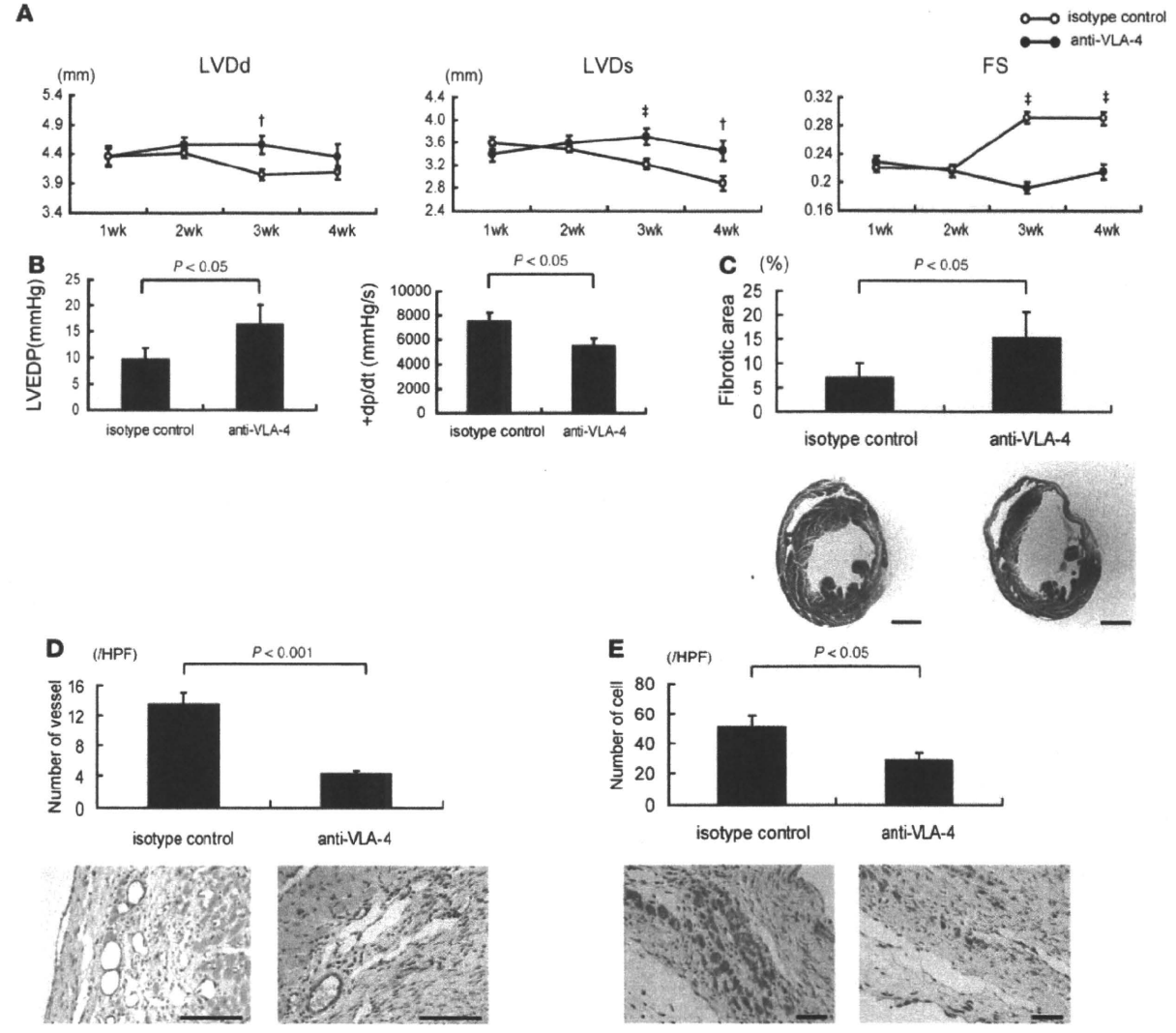

Figure 7

The roles of VLA-4 signaling on CPC sheet transplantation-mediated improved cardiac function. Analysis of cardiac function by echocardiography (**A**, $n = 5$) and catheterization (**B**, $n = 5$). Anti–VLA-4 Ab treatment inhibited the reduction of LVDd, LVDs, and LVEDP and the improvement of FS and +dp/dt by CPC sheet transplantation. Isotype Ab was used as a control. $^{\dagger}P < 0.05$ versus anti–VLA-4 Abs ($n = 5$ per group). $^{\ddagger}P < 0.01$ versus anti–VLA-4 Abs ($n = 5$ per group). (**C**) Masson trichrome staining. The fibrotic area 4 weeks after transplantation was calculated and is shown in the graph ($n = 5$). Anti–VLA-4 Ab treatment inhibited the reduction of fibrotic area following CPC sheet transplantation. Lower panels show representative images. Scale bars: 1 mm. (**D**) vWF staining. The number of vWF-positive vessels in the border area was counted and is shown in the graph ($n = 5$). Anti–VLA-4 Ab treatment inhibited the increased number of vessels in the border area following CPC sheet transplantation. Lower panels show representative images. Scale bars: 100 μm. Nuclei were stained with hematoxylin. (**E**) RFP staining. The number of RFP-positive cells (brown) was counted and is shown in the graph ($n = 5$). Anti–VLA-4 Ab treatment decreased the number of RFP$^+$ cells in the infarcted area following CPC sheet transplantation. Lower panels show representative images. Nuclei were stained with hematoxylin. Scale bars: 100 μm. Data are shown as mean + SEM.

ATMCs were isolated from GFP mice as previously described (48), with a few modifications. In brief, interscapular adipose tissues were digested at 37°C in PBS, which contained 2.5 mg/ml dispase (Invitrogen), for 45 minutes. After filtration through 25-μm filters and centrifugation, isolated ATMCs were suspended in IMDM supplemented with 10% FBS and penicillin/streptomycin/amphotericin B and cultured on 1% gelatin-coated dishes. ATMCs from passages 3–5 were used for cell sheets.

Neonatal rat cardiomyocytes were isolated as previously described (19). Cardiomyocytes were plated at a field density of 1×10^5 cells/cm^2 on 24-well culture dishes (BD Falcon) coated with 1% gelatin and cultured in DMEM supplemented with 10% FBS.

Labeling of cells. Retroviral stocks were generated as previously described (19). CPCs were infected with an RFP-expressing retroviral vector. Infected cells were selected for growth in the presence of neomycin (500 μg/ml) for 2 weeks. Transfection efficiency of RFP was greater than 95%.

Direct cell injection. Within 5 minutes after ligation of the left anterior descending artery, 2.0×10^6 RFP-labeled CPCs were directly injected into the infarcted regions of wild-type mice using a Hamilton syringe.

Cell sheet preparation and transplantation. CPCs or ATMCs were suspended by trypsinization, and the cell suspension (containing 2 ml complete medium) was plated onto a 35-mm temperature-responsive dish grafted with poly(*N*-isopropylacrylamide) (PIPAAm) (Upcell; CellSeed) at 1.0×10^6 cells/dish. The cells were cultured at 37°C. After 5 days in culture, CPCs or ATMCs were incubated on temperature-responsive dishes at 20°C. After 2 hours, CPCs and ATMCs detached spontaneously and floated in the medium as monolayer cell grafts. Wild-type mice were anesthetized by an i.p. injection of 50 mg/kg sodium pentobarbital and ventilated with a volume-regulated respirator. MI was induced by ligation of the left anterior descending artery with a 10-0 Prolene suture. Mice were randomly assigned to 3 groups: mice transplanted with monolayer CPCs (CPC group; $n = 25$); mice transplanted with monolayer ATMCs (ATMC group; $n = 25$); and mice with no transplantation (MI group; $n = 25$). Within 5 minutes of coronary artery ligation, a monolayer cell sheet was placed on a plastic sheet and applied face down onto the surface of the infarcted anterior-lateral region. The plastic sheet was then carefully removed, leaving the monolayer cell sheet over the infarct area without sutures. Ten minutes after transplantation, the chest was closed.

For Ab treatment, anti–VLA-4 Abs (2.5 mg/kg) or anti-rat IgG2bκ Abs (2.5 mg/kg) as control were i.p. injected daily from 2 to 3 weeks following MI or CPC sheet transplantation.

Echocardiography and catheterization. Transthoracic echocardiography was performed with a Nemio 35 ultrasound system (Toshiba) provided with a 12-MHz imaging transducer. For catheterization analysis, the right carotid artery was cannulated under anesthesia by a micropressure transducer with an outer diameter of 0.33 mm (SPR-1000; Millar Instruments), which was then advanced into the LV. Pressure signals were recorded using a Chart5 for Windows data acquisition and analysis system (ADInstruments). Mice were anesthetized with 4% inhaled isoflurane, and the heart rate was maintained at approximately 500 bpm to minimize data deviation during cardiac function measurement.

Flow cytometric analysis. The immunostaining methods have been previously described (4). The percentage of cells expressing each cell surface antigen was analyzed with an EPICS ALTRA flow cytometer using EXPO32 software, version 1.2 (Beckman Coulter).

RNA extraction and RT-PCR. RNA extraction and RT-PCR were performed as described previously (4). Primer sequences are shown in Supplemental Table 1. Real-time PCR amplification was performed in a 7500 real-time PCR system (Applied Biosystems) using GreenER Two-Step qRT-PCR Kit Universal (Invitrogen), according to the manufacturer's instructions. The PCR protocol included an initial denaturation step (95°C, 10 minutes) followed by 50 amplification and quantification cycles (95°C for 15 seconds, 60°C for 60 seconds) and a melting curve program (60–95°C). Relative mRNA expression levels were calculated using the standard curve of pcDNA6.2-GW/EmGFP.

Western blot analysis. Whole-cell lysates (30-50 μg) were resolved by SDS-PAGE. Proteins were transferred to a PVDF membrane (GE Healthcare) and incubated with primary Abs, followed by anti-IgG horseradish peroxidase–conjugated secondary Ab. Specific proteins were detected by enhanced chemiluminescence (GE Healthcare).

Immunohistology. Hearts fixed in 4% PFA were embedded in paraffin, and 4-μm thick sections were cut and stained with Masson trichrome. The extent of fibrosis was measured in 3 sections from each heart, and the value was expressed as the ratio of Masson trichrome–stained area to total LV free wall. Vascularization was examined by measuring the number of endothelial cells in the border zone of hearts 1 and 4 weeks after MI under light microscopy. Endothelial cells were identified by immunohistochemical staining with Abs specific to vWF. Ten random microscopic fields in the border zone were examined, and the number of endothelial cells was expressed as the number of vWF-positive cells/high-power field (original magnification, ×400).

FITC-lectin perfusion assay. At 4 weeks after MI, with or without transplantation of nonlabeled CPC sheet or ATMC sheet, FITC-conjugated *Lycopersicon esculentum* (tomato) lectin (100 μl; Vector Laboratories) diluted in PBS at a concentration of 0.5 mg/ml, was injected into the tail vein of mice under anesthesia. Ten minutes after injection, the animals were perfused with 4% PFA through the LV for 5 minutes. Hearts were removed and post-fixed in 4% PFA at room temperature for 1 hour and subsequently snap-frozen in nitrogen. The fluorescent images were observed by confocal microscopy (LSM710; Zeiss) with LSM software, version 5.0 (Zeiss). Five random microscopic fields in the border zone were examined, and the number of vessels was expressed as the number of lectin-positive vessel/high-power field (original magnification, ×600).

Immunofluorescent staining. The immunostaining methods have been previously described (19). Images were taken by laser confocal microscopy (Radiance2000; Bio-Rad) or fluorescent microscopy (Zeiss) with a CCD camera (Axiocam; Zeiss).

FISH analysis. Monolayer nonlabeled CPC sheets were transplanted onto the surface of the infarcted hearts of wild-type female mice. Four weeks after transplantation, mice were sacrificed, and whole hearts were snap-frozen in nitrogen. Frozen sections were fixed with a mixture of methanol and acetic acid (3:1, v/v) for 90 minutes and subjected to FISH analysis (Cambio). The sections were air-dried and dehydrated by exposure to a graded series of ethanol solutions. They were again air-dried and incubated in 70% formamide at 65°C for 120 seconds, exposed to ice-cold 70% ethanol, and dehydrated in a graded series of ethanol solutions. Nucleotide probes were individually denatured by incubation at 65°C for 10 minutes, followed by 37°C for 60 minutes. Two (30 μl) probes were added to each slide and were hybridized overnight at 37°C. For detection of X and Y chromosomes, FITC- or Cy3-conjugated probes were used, respectively. FITC signal of FITC was amplified using an FITC amplification kit (Cambio). Nuclei were also stained with DAPI. Sections were examined by confocal microscopy (LSM710; Zeiss) and LSM software.

Cytokine Ab array and ELISA. CPCs and ATMCs (1.0×10^6) were seeded onto 10-cm dishes. After incubation for 12 hours in IMDM supplemented with 10% FBS, cells were washed with PBS thoroughly 3 times and medium was changed to serum-depleted IMDM. After incubation for 24 hours in serum-depleted medium, supernatant was collected as CM and contaminated cells were removed using a 0.45-μm filter (BD Falcon). Cytokine release was measured in culture supernatant by cytokine Ab array or ELISA, according to the manufacturer's instructions (RayBiotech Inc. and R&D Systems).

miRNA vector selection and transfection. Sense and antisense oligonucleotide primers (Supplemental Table 2) were designed in conjunction with Invitrogen. These were annealed and cloned into the pcDNA6.2-GW/EmGFP-miR vector (Invitrogen) according to the manufacturer's instructions. All constructs were sequenced to confirm correct insertion of the oligonucleotides. The pcDNA6.2-GW/EmGFP-miR-neg plasmid vector served as a negative control. Each vector was transfected to CPCs using Lipofectamine 2000 (Invitrogen) following the manufacturer's protocol. At 8 hours after transfection, the medium was exchanged. After selecting the appropriate plasmid vector by quantitative RT-PCR on VCAM-1 mRNA expression (Supplemental Figure 9B), that plasmid was transfected into CPCs and CM was collected.

Scratch-wound assay. In vitro "scratch" wounds were established by scraping cell monolayers. Cells were grown on 6-cm dishes, which were previously labeled with a traced line. After injury, the cells were gently washed several times with PBS and incubated with sVCAM-1 (10 nM) or CPC-derived CM. Cell migration from the edge of the injured monolayer was quantified by measuring the distance between wound edges at time of injury and after 24 hours incubation using an inverted phase contrast microscope (Leica) at 5 distinct positions.

Tube-like formation assay. A Matrigel tube formation assay was used to determine the effects of sVCAM-1 (10 nM) and CPC-derived CM on in vitro angiogenesis potential of HUVECs. Growth-factor reduced Matrigel (250 μl; BD Biosciences) was added to each well of a 24-well plate and allowed to polymerize at 37°C for at least 30 minutes. Trypsin-harvested HUVECs (5×10^4) were suspended in 250 μl endothelial basal medium with or without sVCAM-1 or CPC-derived CM and were seeded onto Matrigel. After incubation for 24 hours at 37°C, the cell 2D organization and the network growth area were examined using an inverted phase contrast microscope and were photographed. Tube length was quantified using LAS AF software, version 1.6.1 (Leica).

MTT assay. Neonatal rat cardiomyocytes were cultured in 24-well plates and preincubated with sVCAM-1 (100 nM) or CPC-derived CM for 24 hours in the presence or absence of anti–VLA-4 Abs (5 ng/μl), Akt inhibitor (10 μM), wortmannin (100 nM), SB203580 (10 μM), and PD98059 (10 μM). H_2O_2 (0.2 mM) was added and incubated with the cells for an additional 24 hours. After aspirating the medium, cells were washed with PBS once and 400 μl/well PBS was added. After 2 hours incubation with 5 mg/ml MTT solution, 10% SDS solution was added and incubated overnight. Supernatant OD_{570} was measured.

Apoptosis analysis. Annexin V–Cy3 Apoptosis Detection Kit (Sigma-Aldrich) was used to detect apoptotic CPCs according to the manufacturer's instructions. In brief, 2 days after miRNA plasmid vector transfection, CPCs were incubated with annexin V–Cy3 (1:100) diluted in 1× binding buffer for 5 minutes at room temperature in the dark. The number of annexin V–positive cells relative to GFP-positive cells was counted under fluorescent microscopy.

Statistics. Data are shown as mean ± SEM. Statistical analyses were performed with 2-tailed Student's *t* test for comparisons between 2 groups. Multiple group comparison was performed by 1-way ANOVA followed by Bonferroni's procedure for comparison of means. $P < 0.05$ was considered significant.

Acknowledgments

We thank R. Kobayashi, A. Furuyama, H. Nagao, and K. Yoshihara for their excellent technical assistance. We thank M. Okabe, Osaka University, for the GFP transgenic mice and Shunichi Morikawa, Tokyo Women's Medical University, for his technical advice. This study was supported by a grant-in-aid for Scientific Research on Priority Areas and for Exploratory Research, Ministry of Education, Culture, Sports, Science and Technology: Health (to I. Komuro); the Cell Science Research Foundation and the Takeda Science Foundation (to T. Nagai); Health and Labour Sciences Research grants (to T. Shimizu); a grant-in-aid for Scientific Research, Developmental Scientific Research, and Scientific Research from the Ministry of Education, Science, Sports, and Culture; the Sakakibara Memorial Foundation; the Hisako Yamakawa Award and a Japan Heart Foundation/Novartis Grant for Research Award on Molecular and Cellular Cardiology, 2009, Takeda Science Foundation (to K. Matsuura).

Received for publication September 15, 2008, and accepted in revised form May 27, 2009.

Address correspondence to: Katsuhisa Matsuura, Department of Cardiology, Tokyo Women's Medical University, 8-1 Kawadacho, Shinjuku-ku, Tokyo, 162-8666, Japan. Phone: 81-3-3353-8111; Fax: 81-3-3356-0441; E-mail: mkatu2002@yahoo.co.jp. Or to: Issei Komuro, Department of Cardiovascular Science and Medicine, Chiba University Graduate School of Medicine, 1-8-1 Inohana, Chuo-ku, Chiba 260-8670, Japan. Phone: 81-43-226-2097; Fax: 81-43-226-2096; E-mail: komuro-tky@umin.ac.jp.

1. Dimmeler, S., Zeiher, A.M., and Schneider, M.D. 2005. Unchain my heart: the scientific foundations of cardiac repair. *J. Clin. Invest.* **115**:572–583.
2. Beltrami, A.P., et al. 2003. Adult cardiac stem cells are multipotent and support myocardial regeneration. *Cell.* **114**:763–776.
3. Oh, H., et al. 2003. Cardiac progenitor cells from adult myocardium: homing, differentiation, and fusion after infarction. *Proc. Natl. Acad. Sci. U. S. A.* **100**:12313–12318.
4. Matsuura, K., et al. 2004. Adult cardiac Sca-1-positive cells differentiate into beating cardiomyocytes. *J. Biol. Chem.* **279**:11384–11391.
5. Messina, E., et al. 2004. Isolation and expansion of adult cardiac stem cells from human and murine heart. *Circ. Res.* **95**:911–921.
6. Laugwitz, K.L., et al. 2005. Postnatal isl1+ cardioblasts enter fully differentiated cardiomyocyte lineages. *Nature.* **433**:647–653.
7. Smith, R.R., et al. 2007. Regenerative potential of cardiosphere-derived cells expanded from percutaneous endomyocardial biopsy specimens. *Circulation.* **115**:896–908.
8. Mirotsou, M., et al. 2007. Secreted frizzled related protein 2 (Sfrp2) is the key Akt-mesenchymal stem cell-released paracrine factor mediating myocardial survival and repair. *Proc. Natl. Acad. Sci. U. S. A.* **104**:1643–1648.
9. Cho, H.J., et al. 2007. Role of host tissues for sustained humoral effects after endothelial progenitor cell transplantation into the ischemic heart. *J. Exp. Med.* **204**:3257–3269.
10. Schächinger, V., et al. 2006. Intracoronary bone marrow-derived progenitor cells in acute myocardial infarction. *N. Engl. J. Med.* **355**:1210–1221.
11. Perin, E.C., et al. 2008. Comparison of intracoronary and transendocardial delivery of allogeneic mesenchymal cells in a canine model of acute myocardial infarction. *J. Mol. Cell. Cardiol.* **44**:486–495.
12. Beeres, S.L., et al. 2007. Intramyocardial injection of autologous bone marrow mononuclear cells in patients with chronic myocardial infarction and severe left ventricular dysfunction. *Am. J. Cardiol.* **100**:1094–1098.
13. Zhang, M., et al. 2001. Cardiomyocyte grafting for cardiac repair: graft cell death and anti-death strategies. *J. Mol. Cell. Cardiol.* **33**:907–921.
14. Okano, T., et al. 1993. A novel recovery system for cultured cells using plasma-treated polystyrene dishes grafted with poly (N-isopropylacrylamide). *J. Biomed. Mater. Res.* **27**:1243–1251.
15. Kushida, A., et al. 1999. Decrease in culture temperature releases monolayer endothelial cell sheets together with deposited fibronectin matrix from temperature-responsive culture surfaces. *J. Biomed. Mater. Res.* **45**:355–362.
16. Memon, I.A., et al. 2005. Repair of impaired myocardium by means of implantation of engineered autologous myoblast sheets. *J. Thorac. Cardiovasc. Surg.* **130**:1333–1341.
17. Miyahara, Y., et al. 2006. Monolayered mesenchymal stem cells repair scarred myocardium after myocardial infarction. *Nat. Med.* **12**:459–465.
18. Hida, N., et al. 2008. Novel cardiac precursor-like cells from human menstrual blood-derived mesenchymal cells. *Stem Cells.* **26**:1695–1704.
19. Matsuura, K., et al. 2004. Cardiomyocytes fuse with surrounding noncardiomyocytes and reenter the cell cycle. *J. Cell. Biol.* **167**:351–363.
20. Limana, F., et al. 2002. bcl-2 overexpression promotes myocyte proliferation. *Proc. Natl. Acad. Sci. U. S. A.* **99**:6257–6262.
21. Giancotti, F.G., and Ruoslahti, E. 1999. Integrin signaling. *Science.* **285**:1028–1032.
22. Nakao, S., Kuwano, T., Ishibashi, T., Kuwano, M., and Ono, M. 2003. Synergistic effect of TNF-alpha in soluble VCAM-1-induced angiogenesis through alpha 4 integrins. *J. Immunol.* **170**:5704–5711.
23. Funk, P.E., Stephan, R.P., and Witte, P.L. 1995. Vascular cell adhesion molecule 1-positive reticular cells express interleukin-7 and stem cell factor in the bone marrow. *Blood.* **86**:2661–2671.
24. Garton, K.J., et al. 2003. Stimulated shedding of vascular cell adhesion molecule 1 (VCAM-1) is mediated by tumor necrosis factor-alpha-converting enzyme (ADAM 17). *J. Biol. Chem.* **278**:37459–37464.
25. Satoh, M., et al. 1999. Tumor necrosis factor-α-converting enzyme and tumor necrosis factor-α in human dilated cardiomyopathy. *Circulation.* **99**:3260–3265.
26. Shi, W., et al. 2003. TACE is required for fetal murine cardiac development and modeling. *Dev. Biol.* **261**:371–380.
27. Koch, A.E., Halloran, M.M., Haskell, C.J., Shah, M.R., and Polverini, P.J. 1995. Angiogenesis mediated by soluble forms of E-selectin and vascular cell adhesion molecule-1. *Nature.* **376**:517–519.
28. Chan, B.M., Elices, M.J., Murphy, E., Hemler, M.E. 1992. Adhesion to vascular cell adhesion molecule 1 and fibronectin. Comparison of alpha 4 beta 1 (VLA-4) and alpha 4 beta 7 on the human B cell line JY. *J. Biol. Chem.* **267**:8366–8370.
29. Shai, S.Y., et al. 2002. Cardiac myocyte-specific excision of the beta1 integrin gene results in myocardial fibrosis and cardiac failure. *Circ. Res.* **90**:458–464.
30. Watt, F.M. 2002. Role of integrins in regulating epidermal adhesion, growth and differentiation. *EMBO J.* **21**:3919–3926.
31. Papayannopoulou, T. 2003. Bone marrow homing: the players, the playfield, and their evolving roles. *Curr. Opin. Hematol.* **10**:214–219.
32. Muraski, J.A., et al. 2007. Pim-1 regulates cardiomyocyte survival downstream of Akt. *Nat. Med.* **13**:1467–1475.
33. Purcell, N.H., et al. 2007. Genetic inhibition of cardiac ERK1/2 promotes stress-induced apop-

tosis and heart failure but has no effect on hypertrophy in vivo. *Proc. Natl. Acad. Sci. U. S. A.* **104**:14074–14079.
34. Kwee, L., et al. 1995. Defective development of the embryonic and extraembryonic circulatory systems in vascular cell adhesion molecule (VCAM-1) deficient mice. *Development.* **121**:489–503.
35. Yang, J.T., Rayburn, H., and Hynes, R.O. 1995. Cell adhesion events mediated by alpha 4 integrins are essential in placental and cardiac development. *Development.* **121**:549–560.
36. Urbanek, K., et al. 2006. Stem cell niches in the adult mouse heart. *Proc. Natl. Acad. Sci. U. S. A.* **103**:9226–9231.
37. Hsieh, P.C., et al. 2007. Evidence from a genetic fate-mapping study that stem cells refresh adult mammalian cardiomyocytes after injury. *Nat. Med.* **13**:970–974.
38. Tousoulis, D., et al. 2007. Differences in inflammatory and thrombotic markers between unstable angina and acute myocardial infarction. *Int. J. Cardiol.* **115**:203–207.
39. Zhang, S., et al. 2007. Fusion of human hematopoietic progenitor cells and murine cardiomyocytes is mediated by alpha 4 beta 1 integrin/vascular cell adhesion molecule-1 interaction. *Circ. Res.* **100**:693–702.
40. Wang, X., et al. 2006. The role of the sca-1+/CD31- cardiac progenitor cell population in postinfarction left ventricular remodeling. *Stem Cells.* **24**:1779–1788.
41. Kogata, N., et al. 2006. Cardiac ischemia activates vascular endothelial cadherin promoter in both preexisting vascular cells and bone marrow cells involved in neovascularization. *Circ. Res.* **98**:897–904.
42. Elmadbouh, I., et al. 2007. Ex vivo delivered stromal cell-derived factor-1alpha promotes stem cell homing and induces angiomyogenesis in the infarcted myocardium. *J. Mol. Cell. Cardiol.* **42**:792–803.
43. Qin, G., et al. 2006. Functional disruption of alpha4 integrin mobilizes bone marrow-derived endothelial progenitors and augments ischemic neovascularization. *J. Exp. Med.* **203**:153–163.
44. Urbanek, K., et al. 2005. Cardiac stem cells possess growth factor-receptor systems that after activation regenerate the infarcted myocardium, improving ventricular function and long-term survival. *Circ. Res.* **97**:663–673.
45. Zhu, W., et al. 2008. IGFBP-4 is an inhibitor of canonical Wnt signalling required for cardiogenesis. *Nature.* **454**:345–349.
46. Shimizu, T., et al. 2006. Polysurgery of cell sheet grafts overcomes diffusion limits to produce thick, vascularized myocardial tissues. *FASEB J.* **20**:708–710.
47. Bock-Marquette, I., Saxena, A., White, M.D., Dimaio, J.M., and Srivastava, D. 2004. Thymosin beta4 activates integrin-linked kinase and promotes cardiac cell migration, survival and cardiac repair. *Nature.* **432**:466–472.
48. Planat-Bénard, V., et al. 2004. Spontaneous cardiomyocyte differentiation from adipose tissue stroma cells. *Circ. Res.* **94**:223–229.

Cardiac 12/15 lipoxygenase–induced inflammation is involved in heart failure

Yosuke Kayama,[1,4] Tohru Minamino,[1,2] Haruhiro Toko,[1] Masaya Sakamoto,[3] Ippei Shimizu,[1] Hidehisa Takahashi,[1] Sho Okada,[1] Kaoru Tateno,[1] Junji Moriya,[1] Masataka Yokoyama,[1] Aika Nojima,[1] Michihiro Yoshimura,[4] Kensuke Egashira,[5] Hiroyuki Aburatani,[6] and Issei Komuro[1]

[1]Department of Cardiovascular Science and Medicine, Chiba University Graduate School of Medicine, Chuo-ku, Chiba 260-8670, Japan
[2]PRESTO, Japan Science and Technology Agency, Saitama 332-0012, Japan
[3]Department of Diabetes, Metabolism and Endocrinology and [4]Department of Cardiology, Jikei University School of Medicine, Minato-ku, Tokyo 105-8461, Japan
[5]Department of Cardiovascular Medicine, Graduate School of Medical Sciences, Kyushu University, Higashi-ku, Fukuoka 812-8582, Japan
[6]Genome Science Division, Research Center for Advanced Science and Technology, University of Tokyo, Meguro-ku, Tokyo 153-8904, Japan

To identify a novel target for the treatment of heart failure, we examined gene expression in the failing heart. Among the genes analyzed, *Alox15* encoding the protein 12/15 lipoxygenase (LOX) was markedly up-regulated in heart failure. To determine whether increased expression of 12/15-LOX causes heart failure, we established transgenic mice that overexpressed 12/15-LOX in cardiomyocytes. Echocardiography showed that *Alox15* transgenic mice developed systolic dysfunction. Cardiac fibrosis increased in *Alox15* transgenic mice with advancing age and was associated with the infiltration of macrophages. Consistent with these observations, cardiac expression of monocyte chemoattractant protein 1 (MCP-1) was up-regulated in *Alox15* transgenic mice compared with wild-type mice. Treatment with 12-hydroxy-eicosatetraenoic acid, a major metabolite of 12/15-LOX, increased MCP-1 expression in cardiac fibroblasts and endothelial cells but not in cardiomyocytes. Inhibition of MCP-1 reduced the infiltration of macrophages into the myocardium and prevented both systolic dysfunction and cardiac fibrosis in *Alox15* transgenic mice. Likewise, disruption of 12/15-LOX significantly reduced cardiac MCP-1 expression and macrophage infiltration, thereby improving systolic dysfunction induced by chronic pressure overload. Our results suggest that cardiac 12/15-LOX is involved in the development of heart failure and that inhibition of 12/15-LOX could be a novel treatment for this condition.

CORRESPONDENCE
Issei Komuro:
komuro-tky@umin.ac.jp

Abbreviations used: cDNA, complementary DNA; FS, fractional shortening; HETE, hydroxy-eicosatetraenoic acids; LOX, lipoxygenase; LVDd, left ventricular diastolic dimension; MCP-1, monocyte chemoattractant protein 1; mRNA, messenger RNA; TAC, transverse aortic constriction.

Heart failure is a clinical syndrome that is associated with various cardiovascular diseases such as hypertension and myocardial infarction (Libby and Braunwald, 2008). Comprehensive management using current therapeutic options can markedly reduce the morbidity and mortality of heart failure. Large-scale clinical trials of drugs targeting neurohormonal mechanisms, such as angiotensin-converting enzyme inhibitors and β blockers, have shown that such treatment is effective for reducing mortality in patients with heart failure (Garg and Yusuf, 1995; McMurray, 1999; Goldstein, 2002). However, heart failure is still one of the leading causes of death worldwide (Libby and Braunwald, 2008), so it is important to investigate the underlying mechanisms of this condition and develop more effective treatments.

Arachidonic acid is a free fatty acid that, when liberated from cell membranes, can be metabolized by cyclooxygenase, cytochrome p450, and lipoxygenase (LOX) to form biologically active products such as prostaglandins, leukotrienes, and hydroxy-eicosatetraenoic acids (HETEs;

Y. Kayama, T. Minamino, and H. Toko contributed equally to this paper.

The Rockefeller University Press $30.00
J. Exp. Med. Vol. 206 No. 7 1565-1574
www.jem.org/cgi/doi/10.1084/jem.20082596

The Journal of Experimental Medicine

Kudo and Murakami, 2002). LOXs are a family of lipid-peroxidizing enzymes that oxidize free and esterified polyenolic fatty acids to form the corresponding hydroperoxy derivates (Kuhn and O'Donnell, 2006). The LOX enzymes are named according to the specific carbon atoms of arachidonic acid that are oxidized. Thus, 12/15-LOX is a member of the LOX family that catalyzes the step from arachidonic acid to 12(S)-HETE and 15(S)-HETE (Chen et al., 1994). 12/15-LOX was originally isolated from porcine leukocytes (Yokoyama et al., 1986), but its tissue distribution is now known to be relatively wide, including blood vessels, the brain, and the kidneys (Kuhn and O'Donnell, 2006). Several lines of evidence have suggested that 12/15-LOX may play an important role in the development of atherosclerosis, diabetes, and neurodegenerative disease (Natarajan and Nadler, 2004; Kuhn and O'Donnell, 2006). For example, disruption of the gene for 12/15-LOX in mice significantly reduces the onset of atherosclerosis (Cyrus et al., 1999, 2001; George et al., 2001), whereas an increase of 12/15-LOX expression in mice promotes monocyte–endothelial cell interactions that lead to atherogenesis (Hatley et al., 2003; Reilly et al., 2004; Bolick et al., 2005). Several studies have shown that monocyte 12/15-LOX mediates the oxidative modification of low-density lipoprotein (McNally et al., 1990; Sakashita et al., 1999; Zhu et al., 2003b). An increase of 12/15-LOX activity in vessel walls also contributes to atherogenesis by impairing the macrophage cholesterol efflux pathway (Nagelin et al., 2008). Interestingly, mice with deficiency of 12/15-LOX are resistant to the development of streptozotocin-induced diabetes (Bleich et al., 1999) and autoimmune diabetes (McDuffie et al., 2008). However, there is currently little evidence that 12/15-LOX has a role in heart failure.

In the present study, we showed that cardiac 12/15-LOX induces inflammation that is involved in heart failure. We found that 12/15-LOX expression was markedly increased in the failing heart. Increased expression of this enzyme up-regulates monocyte chemoattractant protein 1 (MCP-1) and promotes the infiltration of macrophages into the heart, thereby causing cardiac fibrosis and systolic dysfunction. Conversely, disruption of *Alox15* reduces cardiac MCP-1 expression and macrophage infiltration, thereby improving systolic dysfunction induced by chronic pressure overload. These findings suggest that inhibition of 12/15-LOX could be a novel treatment for heart failure.

RESULTS

Increased expression of 12/15-LOX causes heart failure

To clarify the molecular mechanisms of heart failure, we performed microarray analysis using cardiac tissue samples obtained from a hypertensive heart failure model (Dahl salt-sensitive rats). Approximately 300 genes showed significant changes of expression in failing hearts compared with control hearts. For example, fetal genes, such as the natriuretic peptide genes and the β-type myosin heavy chain gene, were up-regulated, whereas cardioprotective genes, such as heat shock proteins, were down-regulated (Table S1). Among the genes analyzed, *Alox15* encoding the protein 12/15-LOX was most markedly up-regulated in failing hearts compared with control hearts (Fig. 1 A). Northern blot analysis confirmed that the messenger RNA (mRNA) for this gene was strikingly elevated in heart failure (Fig. 1 B). Immunohistochemistry showed that expression of 12/15-LOX was specifically up-regulated in cardiomyocytes of failing hearts (Fig. 1 C).

To determine whether increased expression of 12/15-LOX could cause heart failure, we established *Alox15* transgenic mice in which expression of the murine *Alox15* gene was under the control of the α-cardiac myosin heavy chain promoter. We obtained two lines of transgenic mice, both of which showed an ~10-fold increase in the myocardial expression of 12/15-LOX compared with their WT littermates (Fig. 2 A; and Fig. S1, A and B). Histological examination also indicated that the transgenic mice showed increased myocardial expression of 12/15-LOX (Fig. 2 B and Fig. S1 C). Consequently, production of 12(S)-HETE and 15(S)-HETE was significantly increased in the hearts of *Alox15* transgenic mice (Fig. 2 C). The left ventricular diastolic dimension (LVDd) was increased and left ventricular fractional shortening (FS) was decreased in *Alox15* transgenic mice from 26 wk of age compared with their WT littermates (Fig. 2 D). These changes observed in the transgenic animals showed further progression with aging (Fig. 2 D). Histological examination revealed that cardiac fibrosis was increased in *Alox15* transgenic mice and that this fibrosis also progressed with advancing age and was associated with infiltration of macrophages (Fig. 2, E and F). There was no difference in blood pressure between *Alox15* transgenic mice and their WT littermates at 16 or 48 wk of age (Fig. S1 D). The cardiac changes were similar in two independent lines of *Alox15* transgenic mice, suggesting that increased expression of 12/15-LOX might cause heart failure by inducing myocardial inflammation.

12/15-LOX induces cardiac inflammation

To investigate the mechanism by which cardiac infiltration of macrophages was increased in *Alox15* transgenic mice, we examined the expression of various proinflammatory cytokines that are thought to be macrophage chemoattractants by the ribonuclease protection assay. We found that cardiac expression of *Ccl2* (MCP-1) was significantly increased in *Alox15* transgenic mice compared with WT mice (Fig. 3 A). In vitro experiments demonstrated that treatment with 12(S)-HETE increased *Ccl2* expression by cardiac fibroblasts and endothelial cells (Fig. 3, B and C), whereas there was no effect when cardiomyocytes were treated with 12(S)-HETE (Fig. 3 D). Moreover, incubation of COS7 cells with 12(S)-HETE significantly increased the activity of nuclear factor κB, a transcription factor that regulates the induction of proinflammatory cytokines including MCP-1 (Fig. 3 E). In contrast, 12(S)-HETE did not affect the activity of this factor when cells were transfected with a reporter plasmid containing mutant κB binding sites (Fig. 3 E). These results suggest that increased production of 12(S)-HETE by cardiomyocytes

causes up-regulation of MCP-1 in other cells of the heart, thereby leading to accumulation of macrophages.

To investigate the relationship between up-regulation of MCP-1 and heart failure, we examined the effect of MCP-1 inhibition on cardiac dysfunction in *Alox15* transgenic mice. We injected an expression vector encoding mutant human MCP-1 with deletion of N-terminal amino acids (7ND plasmid; Egashira, 2003) or the empty vector (mock) into the thigh muscles of mice every 2 wk until 48 wk of age. The result was a significant increase in the blood level of 7ND and elevation of plasma human MCP-1 (Fig. 4 A and Fig. S2). This mutant MCP-1 binds to the MCP-1 receptor (chemokine receptor 2) and inhibits downstream signaling (Egashira, 2003). Consequently, injection of the 7ND plasmid has been reported to suppress MCP-1 activity in vivo and inhibit the development of atherosclerosis (Ni et al., 2001), as well as inhibiting cardiac remodelling after myocardial infarction (Hayashidani et al., 2003). In agreement with these results,

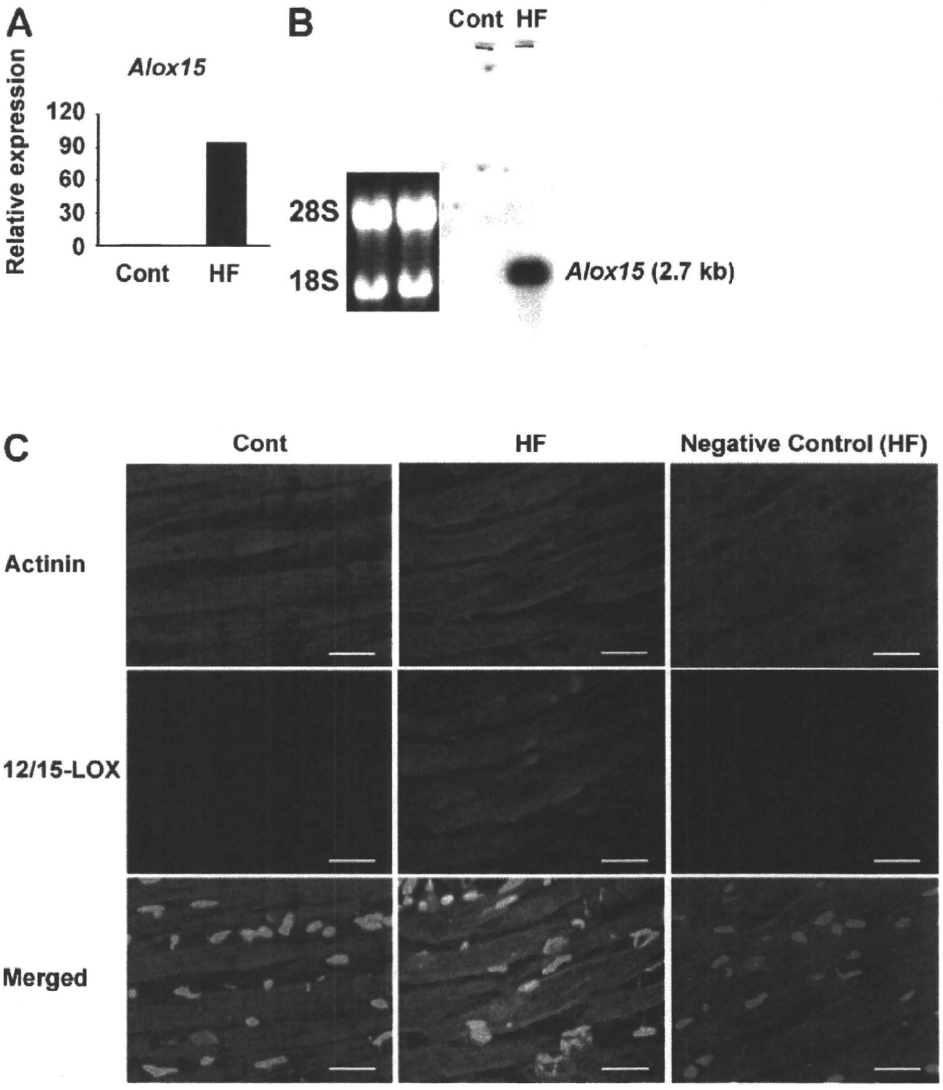

Figure 1. Expression of 12/15-LOX is up-regulated in the failing heart. (A) Dahl salt-sensitive rats were fed a low-sodium diet until the age of 6 wk and then a high-sodium diet (8% NaCl) throughout the experimental period. In this model, prominent cardiac hypertrophy developed and left ventricular systolic function was impaired by 17 wk of age. Rats fed a low-salt diet (0.3% NaCl) served as the control. The animals were sacrificed for gene chip analysis at 17 wk of age. Expression of *Alox15* was markedly up-regulated in failing hearts (HF) compared with control hearts (Cont). (B) Northern blot analysis confirmed that the expression of mRNA for *Alox15* was strikingly elevated in failing hearts. (C) Immunohistochemistry for 12/15-LOX in the heart at 17 wk of age. Expression of 12/15-LOX (red) was specifically up-regulated in cardiomyocytes (green) of failing hearts. Nuclei were stained with DAPI (blue). Bars, 20 µm. Normal rabbit serum was used as a negative control of polyclonal antibody against 12/15-LOX. Results in A are obtained from one experiment. Results in B and C are representative of three independent experiments.